DESIGN, FABRICATION, AND TESTING OF AN ADHESIVE-FREE MOUNT FOR 330 MM TRANSMISSION FLAT OPTICAL WINDOW

by

Bo Wang

A Thesis Submitted to the Faculty of the

JAMES C. WYANT COLLEGE OF OPTICAL SCIENCES

In Partial Fulfillment of the Requirements

For the Degree of

MASTER OF SCIENCE

In the Graduate College

THE UNIVERSITY OF ARIZONA

2022

THE UNIVERSITY OF ARIZONA
GRADUATE COLLEGE

As members of the Master's Committee, we certify that we have read the thesis prepared by **Bo Wang**, titled ***Design, Fabrication, and Testing of an Adhesive-Free Mount for 330 mm Transmission Flat Optical Window*** and recommend that it be accepted as fulfilling the thesis requirement for the Master's Degree.

Professor Daewook Kim Date: 8/12/2022

Professor Brandon D. Chalifoux Date: 8/12/2022

Professor Heejoo Choi Date: 8/12/2022

Final approval and acceptance of this thesis is contingent upon the candidate's submission of the final copies of the thesis to the Graduate College.

I hereby certify that I have read this thesis prepared under my direction and recommend that it be accepted as fulfilling the Master's requirement.

Professor Daewook Kim Date: 8/12/2022
Master's Thesis Committee Chair
Wyant College of Optical Sciences

Table of Contents

List of Figures

List of Tables

Abstract

The manufacturing and testing of optical components has been a mix between a science and an art for the better part of a few thousand years. From the early days of Galileo to the massive polishing laps underneath Arizona Stadium, the design, fabrication, and testing of optical components has contributed to many of the key scientific and technological advancements of humanity. One area that is constantly pushing the limits of optical fabrication, is fabrication for optical metrology equipment such as interferometers. The reference quality optics used in these instruments are pushing the limits of what is possible using traditional optical fabrication techniques such as pitch polishing. The optical substrate is often the most expensive and most critical single component in many systems. Another challenge that goes into the process of building reference quality optics is the need to mount the optic so it can be used with an optical system, such as an interferometer. The design and fabrication of both the mount and the substrate in parallel allows for a most optimal design that will encourage best post assembly performance of the substrate. The mount is an original design that will become a new product line for Precision Optical, a high precision planer components manufacturer located in Costa Mesa California. Design considerations include compensating for the effects of gravity inducing stress on the substrate, the stiffness of the mount, the likelihood of failure analyzed using finite element analysis (FEA) techniques, the best approach for securing the substrate in the mount, and the best fabrication approach for the manufacture of the substrate. Verification was performed using a Zygo ATZ© Fizeau Interferometer, with an 18” beam expander. An overview of the design process for the mount, the fabrication approach, and the verification data is provided. In addition, a large tip-tilt stage that was used in the testing process, but not directly a part of the project itself, was also designed and built. A general overview of the design of the stage is also discussed.

1. Introduction

The development of an efficient and reliably repeatable approach for the fabrication of high precision reference caliber substrates is a major challenge that incorporates a combination of tribal knowledge in addition to proven scientifically developed approaches. The complexity is further increased when the process of assembly of the substrate into a mount is added to the requirements.

The fabrication and assembly of high precision reference quality optical components follow a fundamental set of principles that have been developed over many years, and need to be taken into account in order to reliably produce high quality assemblies. These principles are for optimizing processes that put the substrate in the most ideal position to achieve the necessary surface figure precision needed for reference quality optics. Examples of such principles include stress relieve of the surfaces prior to polishing, acclimation to the environment before final metrology, selection of high homogeneity material, and many other considerations.

Because the order of magnitude for many of the specifications is on the scale of nanometers to in order to produce a successful reference quality assembly. The fabrication process approach is most critical in the production of the substrate, and precise opto-mechanical considerations for the design of the mount need to be accounted for. This makes the entire endeavor not one to be taken trivially, as the combination of these considerations need to work in sync to produce a successful mounted transmission flat.

Precision Optical is a high precision planer-components manufacture located in Costa Mesa California. It has been in continuous operation for over 60 years, and is a world leader in the manufacturer of tight tolerances flats, prisms, coatings, and assemblies. The company employs 70 employees, and has been producing reference quality optics for customers around the world

for several decades. Specializing in traditional single-pitch polishing along with state-of-the-art metrology equipment which include two Zygo ATZ 18” Interferometers, five coating chambers capable of coating sizes up to 480mm in diameter, as well as an internal machine shop with three and five axis capabilities for the fabrication of metal components. This makes Precision Optical an ideal supplier for assemblies such as the one being described by this paper.

This paper present and overview of design and fabrication of a 330mm Mounted Transmission Flat designed to be used with a Zygo (or other custom designed) beam expander system. In addition, a large tilt stage was also made in order to set components on to null out fringes during measurement. This paper will give an overview of the design and fabrication process of the transmission flat, an overview of the design decisions on the mount, an overview of the assembly process, as well as the metrology used to certify the flat prior to customer delivery. The areas that require the most risk assessment will be examined, and a detailed overview of the optomechanical and process design will be described.

2. Technical Overview

The following is a technical overview of the concepts of are being explored in this project. The concepts span from a high-level view of interferometry, to the design consideration that are needed to take place for the design of the opto-mechanical mount, an overview of optical fabrication, an overview of metrology procedures. All of these directly and in-directly contribute to the design and manufacturing of the opto-mechanical mount and the transmission flat.

2.1 Fundamentals of Interferometry

When the discovery of the fact light behaves as a wave, the phenomenon of light interference was seen as a method to make sensitive measurements, and thus was born the technique of two-beam interference for high precision scientific research and measurements. Among the world’s

most precise measurement instruments are based on interferometric theory. One such example is the Laser Interferometer Gravitational-Wave Observatory (LIGO), which is a Michelson Interferometer that is being used in the search for gravitational waves.[1]

In its most basic form, interferometry is the combination of two waves. Light, being electromagnetic radiation, is described as a superposition of plane waves.

Two plane waves traveling in space can be represented as:

$$U_1(r,t) = A_1\left(a_{x1}\hat{x}+a_{y1}\hat{y}+a_{z1}\hat{z}\right)e^{[j(k_1\cdot r-\omega_1 t)]} \quad (1)$$

$$U_2(r,t) = A_2\left(a_{x2}\hat{x}+a_{y2}\hat{y}+a_{z2}\hat{z}\right)e^{[j(k_2\cdot r-\omega_2 t)]} \quad (2)$$

Where:

$$\hat{a} = a_x\hat{x} + a_y\hat{y} + a_z\hat{y} \quad (3)$$

Is the polarization vector (Eq. 3).[2] When the two waves represented by (Eq. 1) and (Eq. 2) are linearly added in space (assuming both have the same polarization components) you have the result:

$$U_1(r,t) + U_2(r,t) = A_1\left(a_{x1}\hat{x}+a_{y1}\hat{y}+a_{z1}\hat{z}\right)e^{[j(k_1\cdot r-\omega_1 t)]} +$$

$$A_2\left(a_{x2}\hat{x}+a_{y2}\hat{y}+a_{z2}\hat{z}\right)e^{[j(k_2\cdot r-\omega_2 t)]} \quad (4)$$

In order to simplify, we use the trigonometric identity

$$\cos A \cos B = 2\cos\left(\frac{A+B}{2}\right)\cos\left(\frac{A-B}{2}\right) \quad (5)$$

And thus (Eq. 4) reduces to

$$(r,t) = 2A_y\cos\left(\frac{1}{2}(k_1\cdot r-\omega_1 t)\right)\cos\left(\frac{1}{2}(k_2\cdot r-\omega_2 t)\right) \quad (6)$$

[1] Milster T. (2017) Interference and Interferometry OPTI 505R Diffraction and Interferometry . Ch. 4, 4-7

[2] Milster T. (2017) Interference and Interferometry OPTI 505R Diffraction and Interferometry . Ch. 4, 4-8

The addition of these two plane waves represented by (Eq. 6) results in the creation of interference fringes.

Fringes are created when copies of wave are created in which the shape remains the same. Interferometers are generally classified into two types, 1) division of wavefront, when they are usually in the form of pinholes and slits, where the points/slits produce new wavefronts from those points such as shown in (See Fig. 1)[3];

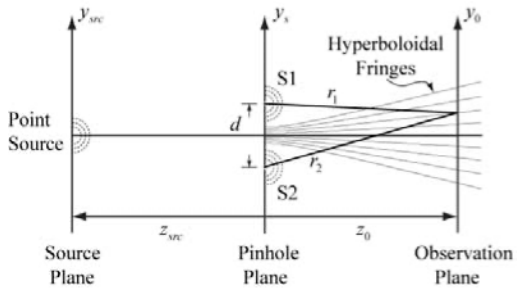

Figure 1: Example of a division of wavefront interferometer in the form of a pinhole from ©Tom D. Milster 2017, Chapter 4: Interference and Interferometry

And 2) Division of amplitude, such as the parallel plate setup, which is a technique that is widely used in optical fabrication to perform spot checks on optical components during the polishing process. A light source (usually monochromatic) is positioned at a distance *l* and is reflected from the surfaces of two plates stacked on top of each other.[4] The reflection from the front surface of the refracts onto the plate, and then reflects off the back surface such as shown in (See Fig. 2). The wave finally exits the front again, it appears to come from the backplate. The coherent point-source that is generated by the reflections is separated by a distance *d*. Defined by

$$d = \frac{2t}{n} \tag{7}$$

[3] Milster T. (2017) Interference and Interferometry OPTI 505R Diffraction and Interferometry . Ch. 4, 4-8
[4] Milster T. (2017) Interference and Interferometry OPTI 505R Diffraction and Interferometry . Ch. 4, 4-57

Where *n* is the index of refraction of the glass and *t* is the thickness/distance between the two surfaces as used in (Eq. 7). The result is the generation of interference fringes, appearing as sequential light and dark lines.

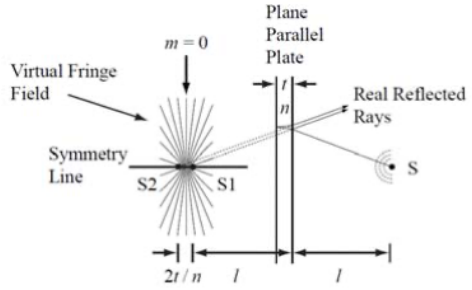

Figure 2: Layout of a basic parallel plate interferometer set up. ©Tom D. Milster 2017, Chapter 4: Interference and Interferometry

This division of amplitude interferometric process can also be represented in the form of two parallel plates with a wedge in-between the two of them as shown in (See Fig. 3). This setup is known as a Fizeau interferometer.[5]

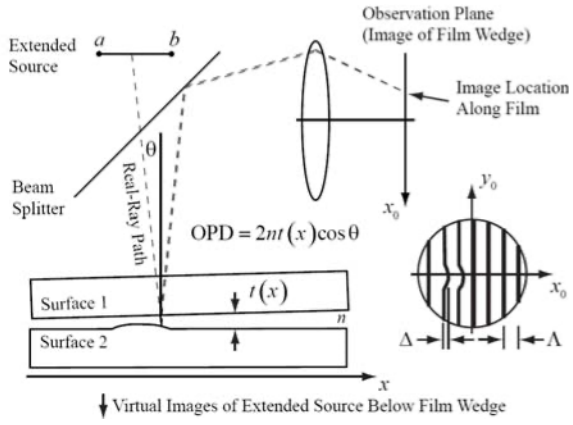

Figure 3: Layout of a Fizeau interferometer. ©Tom D. Milster 2017, Chapter 4: Interference and Interferometry

[5] Milster T. (2017) Interference and Interferometry OPTI 505R Diffraction and Interferometry . Ch. 4, 4-57

A wedge is formed between the two surfaces (the bottom of the top plate and the top of the bottom plate), where the top plate is a reference flat. Light from a source (typically monochromatic when in a shop environment) reflects off the surface of the optic being tested, and creates straight fringes on the surface of the reference optic. The straight fringes indicate that the surfaces are uniform, however if there is a curve in the fringes, it is an indication of a defect, or an object that is in-between the two plates created a wedge. In the area of the defect, the fringes move to position of equal optical path difference (OPD) towards the higher side of the wedge. The OPD between the reflections from the defect determines the shape of the fringes that appear on the reference optic, and is represented by (Eq. 8)[6].

In normal incidence where $\theta = 0$ and $n = 1$, the OPD is

$$OPD(x) = 2t(x) \tag{8}$$

Where each fringe is half a wavelength of the thickness change. This process is regularly used in an optical shop environment to check flatness of planer optical components during the polishing process as shown in (See Fig. 4).[7]

[6] Milster T. (2017) Interference and Interferometry OPTI 505R Diffraction and Interferometry . Ch. 4, 4-58
[7] Milster T. (2017) Interference and Interferometry OPTI 505R Diffraction and Interferometry . Ch. 4, 4-59

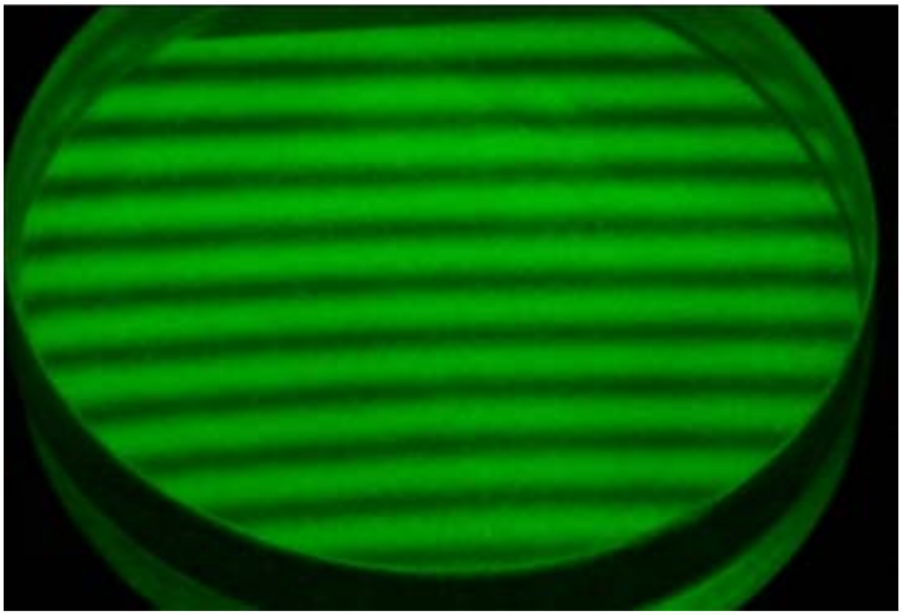

Figure 4: Fizeau fringes visible on a test plate. ©Tom D. Milster 2017, Chapter 4: Interference and Interferometry

This technique has been used by optical shops for generations, however with the advent of laser interferometers, the techniques that have been relied upon have been greatly enhanced with modern equipment, and has become among the most precision optical metrology equipment available today in the form of laser Fizeau interferometers.

2.2 Basics of Fizeau Interferometry

Fizeau Interferometry (or the use of a fizeau laser interferometry) is an interferometer that is arranged where two reflecting surfaces are facing one another. They are often used to measures the surface figure and transmission quality of specular (polished) optical grade surfaces. This is achieved when the light reflected from the rear surfaces of the first optics is combined with the

light from the front surface of the second optic to produce interference fringes.[8] In the case of a fizeau laser interferometer, a beam-splitter divides the beam from a laser source (See Fig 5).

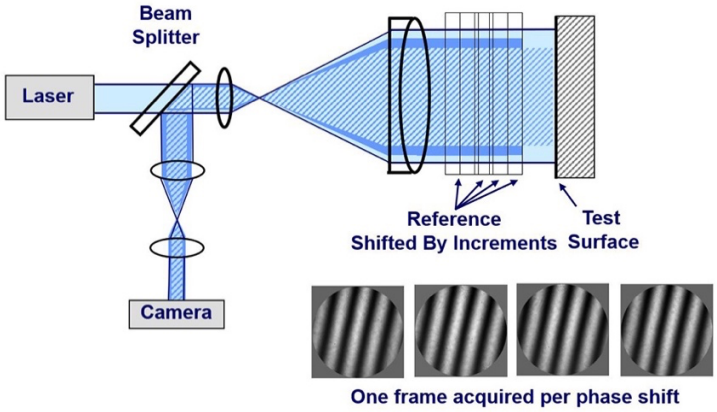

Figure 5: General Layout of 4D Accufiz® Fizeau Interferometer

The 'reference' beam is directed at a high-quality surface (such as a reference quality transmission flat), and the 'test' beam is directed at the surfaces that is being tested, or through a test optic to a high-quality return mirror. The resulting phenomenon is in the form of fizeau fringes, which is an interference pattern that is the result of the interference of the two beams that occurs near a thin layer.[9]

Fizeau laser interferometers have been developed to the point that there are many iterations of the technology, including ever expanding sizes of the reference flat have allow the ability to expand the reference beam to larger sizes, in some cases up to 1 meter in diameter. In addition, companies such as 4D Technology, located in Tucson AZ, have developed dynamic phase

[8] Milster T. (2017) Interference and Interferometry OPTI 505R Diffraction and Interferometry . Ch. 4, 4-58
[9] Milster T. (2017) Interference and Interferometry OPTI 505R Diffraction and Interferometry . Ch. 4, 4-58

shifting fizeau interferometry, in which the reference surface is motioned relative to the test surface, and the instrument acquires data at each position point.[10]

This setup allows for the operator to measure features such as wavefront error and surface height. Although most phase shifting interferometers needs to be isolated from vibration such as being placed on an air table, dynamic phase-shifting interferometers are able to isolate the vibration, thus allowing it to be placed in manufacturing environments, greatly improving in-process metrology of optical components.

2.2 Basics Opto-Mechanical Principles

There are a number of fundamental consideration when designing a system and/or assembly. Such considerations include 1) selection of material 2) effects of temperature changes on the system 3) stress and strain considerations for the assembly 4) appropriate mounting techniques and procedures 5) effects of friction and gravity acting on the assembly.

2.2.1 Calculation of Stiffness

When an optic is mounted in any orientation, gravity acts on it and causes deformation (in addition to displacement as described above) due to the force due to grave ("mg"); this is known as self-weight deflection, which is a common concern when mounting a mirror.[11] The rms self-weight deflection can of a mirror mounted laterally (axis horizontal) at 45-degree rotations, can be estimated by:

$$\delta_{Hrms} = (a_0 + a_1\gamma + a_2\gamma^2)\left(\frac{2\rho r^2}{E}\right) \quad (9)$$

[10] 4D Technology (n.d.) Dynamic Interferometry Retrieved October 14, 2021 from https://4dtechnology.com/products/dynamic-interferometry/

[11] Schwertz, K., & Burge, J. (2012). Large-Mirror Mounting: Active Supports. In *Field Guide to Optomechanical Design and Analysis* (Vol. FG26, Ser. SPIE Field Guides, pp. 82–83). essay, SPIE Press.

where:

$$\gamma = \left(\frac{r^2}{2hR}\right) = \left(\frac{Sag}{Thickness}\right) \tag{10}$$

Where 'a' is the Schwesnger factor for a two-point support geometry when calculating the sag due to gravity[12] C_k for horizontally mounted circular mirrors. Although this equation is used for a V-type mount that isn't the exact same geometry as our design, and assumption was made that since both designs are horizontally mounted with two points-of-contact clocked at 45 degrees that this equation for deformation would be a close enough approximation[13]. This is needed to determine the stiffness of the system as a whole, as the deformation would technically result in the clear aperture to move from a theoretical perfect circle, to an ellipse when the deformation is accounted for. This change is needed to be noted in order to see if the sag will have any meaningful effect on the system.[14]

2.2.2 Finite Element Analysis

In any mechanical system, another force that needs to take into consideration is defining them as stress and strain. By definition, stress occurs when an object is subjected to a force, simply defined as a force divided by the cross-sectional area the force is impinging on. Strain is when an object is subject to an axial force, which changes the length dimensionally of an optic. It is represented as a ratio between the length of the object to the original length. To evaluate the

[12] Schwertz, K., & Burge, J. (2012). Large-Mirror Mounting: Active Supports. In *Field Guide to Optomechanical Design and Analysis* (Vol. FG26, Ser. SPIE Field Guides, pp. 82–83). essay, SPIE Press.

[13] Yoder, P. (2015). In D. Vukobratovich (Ed.), *Opto-Mechanical Systems Design DESIGN AND ANALYSIS OF LARGE MIRRORS AND STRUCTURES* (4th ed., Vol. 2, pp. 121–122). essay, CRC Press.

[14] Yoder, P. (2015). In D. Vukobratovich (Ed.), *Opto-Mechanical Systems Design DESIGN AND ANALYSIS OF LARGE MIRRORS AND STRUCTURES* (4th ed., Vol. 2, pp. 121–122). essay, CRC Press.

design further in addition to tolerance analysis to ensure fit and finish, a Finite Element Analysis is performed on a CAD model.[15]

Finite Element Analysis (FEA) is a method to simulate physical phenomenon using a technique called the Finite Element Method (FEM). FEA Software is used to build models of physical systems virtually, and is used to analyze and determine short comings early, without the need to build multiple prototypes.[16] Using mathematics, we can understand and models various phenomena wave propagation stray light analysis. These processes are often described using Partial Differential Equations (PDEs). Finite Element Analysis is used by computers to solve these PDEs to help researchers and scientist to model phenomenon, and in this case structural and mechanical analysis.[17]

Differential equations are regularly used to describe both natural phenomena and physical phenomena in engineering. Partial Differential Equations (PDEs) are equations that are used to solve certain quantities of structures (like stresses (σ), strains (ϵ), etc.) in order to model their behavior when under a load such as force due to gravity. In the case of this mount, FEA is a mathematical method that is used to predict of how this opto-mechanical assembly behaves under our given conditions. We use it to find things like weak spots and areas of tension in our

[15] *What is FEA: Finite element analysis? documentation*. SimScale. (2021, September 2). Retrieved August 14, 2022, from https://www.simscale.com/docs/simwiki/fea-finite-element-analysis/what-is-fea-finite-element-analysis/

[16] Schwertz, K., & Burge, J. (2012). Finite Element Analysis. In *Field Guide to Optomechanical Design and Analysis* (Vol. FG26, Ser. SPIE Field Guides, pp. 90–91). essay, SPIE Press.

[17] *What is FEA: Finite element analysis? documentation*. SimScale. (2021, September 2). Retrieved August 14, 2022, from https://www.simscale.com/docs/simwiki/fea-finite-element-analysis/what-is-fea-finite-element-analysis/

design. The results of a simulation-based on the FEA method are usually depicted via a color scale that shows, for example, the pressure distribution over the object.[18]

2.2.2.1 Von Mises Analysis

When a body is in an initial state of equilibrium (or undeformed state), is under the influence of a force, the body deforms correspondingly until it reaches a new state of equilibrium. In the case of the mount, the internal forces are the result of the force due to gravity, while the surface forces are the result of the flat and resting on the engagement pads while in contact with the rubber. The relations between the force due to gravity in the form of stress and the deformation in the form of strain, is commonly known as "Stress-Strain" relations (See Fig. 6)[19].

The 'elastic limit' refers to the region where energy is not lost during the stress/strain process, i.e., the processes that do not exceed the elastic limit are reversible. This is also known as yield stress. When a system is above that limit, the deformations go from being elastic and become plastic, and thus are irreversible. The stress of the elastic limit is defined here as Sy.[20]

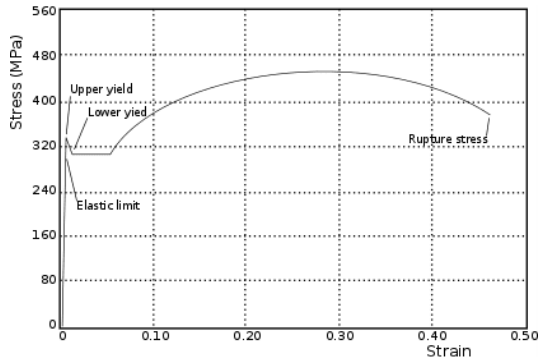

[18] *What is FEA: Finite element analysis? documentation*. SimScale. (2021, September 2). Retrieved August 14, 2022, from https://www.simscale.com/docs/simwiki/fea-finite-element-analysis/what-is-fea-finite-element-analysis/

[19] *What is von mises stress in fea?: SimWiki*. SimScale. (2021, September 2). Retrieved August 14, 2022, from https://www.simscale.com/docs/simwiki/fea-finite-element-analysis/what-is-von-mises-stress/

[20] *What is von mises stress in fea?: SimWiki*. SimScale. (2021, September 2). Retrieved August 14, 2022, from https://www.simscale.com/docs/simwiki/fea-finite-element-analysis/what-is-von-mises-stress/

Figure 6: Common approximation for the stress-strain plot generalized for all the materials when under uniaxial tension.

As discussed before, the elastic limits are based on simple tension or uniaxial stress experiments. The maximum distortion energy theory, however, originated when it was observed that materials, especially ductile ones, behaved differently when a non-simple tension or non-uniaxial stress was applied, exhibiting resistance values that are much larger than the ones observed during simple tension experiments. A theory involving the full stress tensor was therefore developed.

The von Mises stress is a criterion for yielding, and is widely used for metals and other ductile materials. It states that yielding will occur in a body if the components of stress acting on it are greater than the criterion[21]:

$$\frac{1}{6}[(\tau_{11}-\tau_{22})^2 + (\tau_{22}-\tau_{33})^2 + (\tau_{33} - \tau_{11})^2 + 6(\tau_{12}^2 + \tau_{23}^2 + \tau_{13}^2)] = k^2 \quad (11)$$

The constant k is defined through experiment and τ_{ij} is the stress tensor components. Common experiments for defining k are made from uniaxial stress, where the above expression reduces to:

$$\frac{\tau_y^2}{3} = k^2 \quad (12)$$

If τy reaches the simple tension elastic limit, Sy, then the above expression becomes:

$$\frac{S_y^2}{3} = k^2 \quad (13)$$

[21] *What is von mises stress in fea?: SimWiki*. SimScale. (2021, September 2). Retrieved August 14, 2022, from https://www.simscale.com/docs/simwiki/fea-finite-element-analysis/what-is-von-mises-stress/

Which can be substituted into the first expression:

$$\frac{1}{6}[(\tau_{11-}\tau_{22})^2 + (\tau_{22} - \tau_{33})^2 + (\tau_{33} - \tau_{11})^2 + 6(\tau_{12}^2 + \tau_{23}^2 + \tau_{13}^2)] = \frac{S_y^2}{3} \quad (14)$$

or, finally

$$\sqrt{\frac{(\tau_{11-}\tau_{22})^2+(\tau_{22-}\tau_{33})^2+(\tau_{33-}\tau_{11})^2+6(\tau_{12}^2+\tau_{23}^2+\tau_{13}^2)}{2}} = S_y \quad (15)$$

The von Mises stress, τv, is defined as:

$$\tau_v^2 \geq S_y \quad (16)$$

Therefore, the von Mises yield criterion can be rewritten as:

$$\tau_v \geq S_y \quad (17)$$

This shows that if the von Mises stress is greater than the simple tension yield limit stress, then the material will likely yield. Note that von Mises stress is not a true stress, it is a theoretical value that allows the comparison between the general tridimensional stress with the uniaxial stress yield limit., also known as the octahedral yield criterion.[22]

Which, for the case of uniaxial or simple tension, simplifies to:

$$\sqrt{(\tau_1-\tau_2)^2(\tau_2 - \tau_3)^2 + (\tau_3 - \tau_1)^2} = \tau_{oct} \quad (18)$$

[22] *What is von mises stress in fea?: SimWiki*. SimScale. (2021, September 2). Retrieved August 14, 2022, from https://www.simscale.com/docs/simwiki/fea-finite-element-analysis/what-is-von-mises-stress/

Again, if τy reaches the simple tension elastic limit, Sy, then the above expression becomes:

$$\frac{\sqrt{2}}{3}\tau_y = \tau_{oct} \tag{19}$$

And thus, you get the octahedral stress expression:

$$\frac{\sqrt{2}}{3}S_y = \tau_{oct} \tag{20}$$

If the octahedral stress is greater than the simple stress yield limit, then yield is expected to occur.[23] The von Mises stress in our example, be applied to our transmission flat assembly, where the engagement pads are expected to be under pressure and combined loading conditions. In these cases, like this, the von Mises stress can be written as:

$$\sqrt{\frac{(\tau_z-\tau_t)^2(\tau_t-\tau_r)^2+(\tau_r-\tau_z)^2}{2}} = \tau_v \tag{21}$$

Where z, r, and t are the axial, radial and tangential stresses. The criterion is the same as before, that is, if the von Mises stress obtained from the above expression is equal or greater than the simple tension yield stress of the material, then yielding is expected to occur. In our case a FEA analysis was done on the mount which resulted in the following results for von Mises Stress with respect to gravity[24].

2.2.3 Calculating Natural Frequency

Another consideration goes into the fact that the system as a whole has a natural frequency, with the spring acting as an oscillator and the vibration pads becoming a form of damping. Natural

[23] *What is von mises stress in fea?: SimWiki*. SimScale. (2021, September 2). Retrieved August 14, 2022, from https://www.simscale.com/docs/simwiki/fea-finite-element-analysis/what-is-von-mises-stress/

[24] *What is von mises stress in fea?: SimWiki*. SimScale. (2021, September 2). Retrieved August 14, 2022, from https://www.simscale.com/docs/simwiki/fea-finite-element-analysis/what-is-von-mises-stress/

frequency is the rate at which an object vibrates when it is disturbed (e.g., plucked, strummed, or hit). A vibrating object may have one or multiple natural frequencies. Simple harmonic oscillators can be used to model the natural frequency of an object.[25]

Simple harmonic oscillators can be used to model the natural frequency of a system. A simple example of a simple harmonic oscillator is a ball on the end of a spring. If this system has not been disturbed, it is at its equilibrium position – the spring is partially stretched out due to the weight of the ball. Applying a force to the spring, like pulling the ball downward, will cause the spring to start oscillating, or go up and down, about its equilibrium position.[26]

In our case, we have a more complicated harmonic oscillators can be used to describe other situations, such as if the vibrations are "damped" slow down due to friction. This type of system is more applicable to the engagement pad system that we have in this mount, with the spring acting as the oscillator, and the vibration pads adding as the damper.

The total equation for the system would be:

$$\frac{d^2x}{dt^2} + 2\zeta\omega_n\frac{dx}{dt} + \omega_n^2 x = 0 \tag{22}$$

Where:

$$\omega_0 = \sqrt{\frac{k}{m}}$$

In our case, the natural frequency of our system would be:

$$f = \frac{\omega}{2\pi} \tag{23}$$

[25] Schwertz, K., & Burge, J. (2012). Vibration. In *Field Guide to Optomechanical Design and Analysis* (Vol. FG26, Ser. SPIE Field Guides, pp. 94–95). essay, SPIE Press.

[26] Schwertz, K., & Burge, J. (2012). Vibration. In *Field Guide to Optomechanical Design and Analysis* (Vol. FG26, Ser. SPIE Field Guides, pp. 94–95). essay, SPIE Press.

Where:

$$\omega_0 = \sqrt{\frac{k}{m}} \tag{24}$$

The damping ratio would be:

$$\zeta = \frac{c}{2\sqrt{mk}} \tag{25}$$

Where:

Table 1. System Damping Ratio Conditions

$\zeta < 1$	Underdamped
$\zeta = 1$	Critically Damped
$\zeta > 1$	Overdamped

Where:

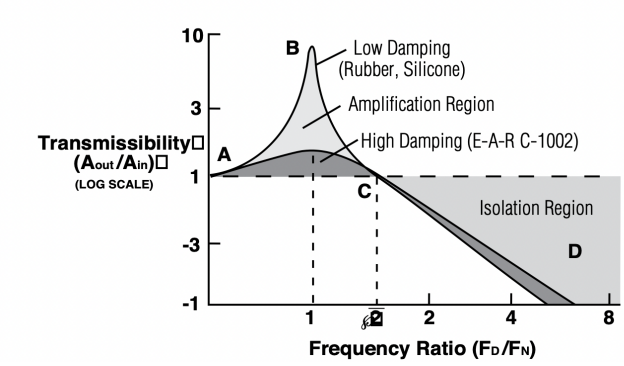

Figure 7. Two typical transmissibility curves, one for a highly damped material (ζ≈0.5), another for a material with much lower damping (ζ≈ 0.05)[27]

[27] Steidel (1971). *An Introduction to Mechanical Vibrations*. John Wiley & Sons. p. 37. *damped*, which is the term used in the study of vibration to denote a dissipation of energy

The ultimate goal is to have the damping frequency is to damp out any affects that would affect the system as the result of the natural frequency of the system. However, when examining the environmental and perturbation frequencies, there are within a +/- 5X range of the natural frequency of the system, rendering the any effect due to these frequencies negligible. [28]

2.5 Overview of Optical Fabrication

The fabrication of high precision optics has been a highly developed field of trial and error that has matured over the last couple hundred years. Going back over 3600 years to the birth of glass making, to the days of Ancient Greece when the first concepts of optical components appeared, the field of optical fabrication is one that is constantly improving, never to be fully mastered.

2.5.1 Types of Optical Fabrication Techniques

In general, there are two schools of thought when approaching the manufacturing of high precision optical components, either the tradition grinding and polishing method that result in unique components, or a replication method that produces near identical parts over and over again.[29]

Optical fabrication in many ways, is still a traditional art whose methods have been handed down through apprentice style training over generations. Traditional pitch polishing, such as the one used to produce this reference quality transmission flat, has been used for over a hundred years, and is still producing many high precision components today.[30] This technique is based on a traditional shaping, grinding, polishing method, which has the ability to produce very high

---

[28] Steidel (1971). *An Introduction to Mechanical Vibrations*. John Wiley & Sons. p. 37. *damped*, which is the term used in the study of vibration to denote a dissipation of energy

[29] Gregory M. Sanger, "Optical Fabrication Technology, The Present and Future," Proc. SPIE 0433, Contemporary Methods of Optical Manufacturing and Testing, (9 December 1983); https://doi.org/10.1117/12.936782

[30] Brown, N. J. "Optical polishing pitch," Preprint UCRL-80301 (Lawrence Livermore National Laboratory, 1977).

precision optical components such as lenses, windows, mirrors, prisms, and more. The drawback of these tradition methods is that they are very labor intensive, and every step of the process has a long learning curve in order to master. It is not uncommon for it taking a decade plus of training and experience before a technician can become a master of the polishing process. However, this technique is also the most likely to produce the most high-quality components in terms of surface figure, surface quality, and subsurface damage. Along with modern metrology equipment such as laser interferometers and coordinate measuring machines (CMM), the limits of what can be achieve is limited to by how precise specification can be measured in process. Advancements in the field of optical fabrication has led to more repeatable results and replication. One of these advancements is the introduction of computer-numeric-control (CNC) optical component generators, that greatly reduces the labor and of individuals technicians. This is due in part that the learning curve for the use of CNC machines, such as automated lens generators produced by companies such as Satisloh and OptiPro. However, the skill and experience of the technician, even with advanced tools such as these CNC machines, will produce better components overall. These machines have the advantage in that they can produce repeatable components at a faster rate, which is optimal when it comes to building catalogue components. However, a drawback is that the surface figure and surface quality of the components have their limits, which can potentially restrict the use for building optical components for semi-conductor and high-powered laser applications.

2.6 Overview of Optical Metrology

A key component to the manufacturing process is the metrology process to verify speciation's and tolerances during the manufacturing process. Metrology is performed in situ when fabricating optical components, as tight tolerances are needed to produce high performance, and

in our case, reference quality optics. Metrology can generally be divided into two categories, mechanical, and optical.

Mechanical metrology is in the form of examining physical dimensions, such as length, width, thickness, and angular considerations. Drop gauges, CMMs, and Goniometers are often used to determine whether these dimensions are within tolerance. One area that blurs the line between optical and mechanical metrology is when angular tolerances for planar components such as prism and flats are being measured, such as beam deviation and parallel. This is because the beam deviation will be affected by material properties and surface characteristics. The index of refraction will contribute to the set-up of autocollimators in the testing process, and improper measurements can result if the set-up doesn't into account the refractive effect of the glass including the homogeneity of the material. In addition, the surface figure of the polished surfaces can also have an effect on the angular measurements. When needing deviation measurements in the range of less than an arc second, the irregularity of the surfaces of planar components, such as ultra-parallel windows, the slight curvature of the surfaces (depending on the thickness of the optic) could produce enough of a deviation that would need to be compensated for in the measurements.[31]

This leads to the need to add the optical metrology to be incorporated into the quality assurance process. Even though it might be possible to measure surface figure using mechanical measurements on a drop gauge or CMM, the results are not accurate enough to infer conclusions of the surface figure and wavefront error of the optic. This is where the need for high precision interferometers to be introduced. Use the theoretical techniques of two-beam interference

[31] W. Osten, "Optical metrology: the long and unstoppable way to become an outstanding measuring tool," Proc. SPIE 10834, Speckle 2018: VII International Conference on Speckle Metrology, 1083402 (7 September 2018);https://doi.org/10.1117/12.2322533

discussed earlier, can produce far more accuracy results for specifications such as surface figure, and angular displacement. When working with reference quality optics, i.e., and optic that will be eventually used to perform metrology on other optical components, often times the highest precision will be needed in order to ensure that high confidence in the measurements.

2.6.1 Interpretation of Zernike Polynomials

A key component of the usefulness of interferometric measurements are Zernike polynomials, which are a mathematical representation that is key to help define different surface figures in interferometric metrology. Zernike polynomials were first formulated by Fritz Zernike in the 1930's. These polynomials are in the form of two variables, ρ and θ, that orthogonal over a unit circle (See Fig. 8)[32].

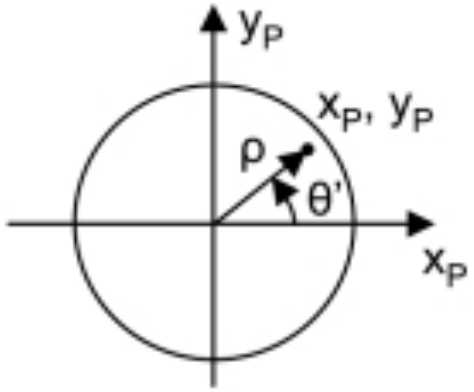

Figure 8: Layout of a unit circle.[33]

Where:

$$x_P = \rho \cos(\theta)' \tag{26}$$

$$y_P = \rho \sin(\theta)' \tag{27}$$

$$\rho = \sqrt{x_P + y_P} \tag{28}$$

[32] Goodwin, E. P., & Wyant, J. C. (2006). *Field Guide to Interferometric Optical Testing*. SPIE Press.
[33] Goodwin, E. P., & Wyant, J. C. (2006). *Field Guide to Interferometric Optical Testing*. SPIE Press.

These polynomials are used to interpret wavefront data and are useful to express various optical aberrations.

Table 2. List of Zernike Polynomials and Aberrations

Order	Function	Aberration
1	1	Piston
2	$\rho \sin(\theta)$	Tilt-Y
3	$\rho \cos(\theta)$	Tilt-X
4	$\rho^2 \sin(2\theta)$	Astigmatism 1st order 45°
5	$2\rho^2 - 1$	Defocus
6	$\rho^2 \cos(2\theta)$	Astigmatism 1st order 0°
7	$\rho^3 \sin(3\theta)$	Trefoil 30°
8	$(3\rho^3 - 2\rho) \sin(\theta)$	Coma-Y
9	$(3\rho^3 - 2\rho) \cos(\theta)$	Coma-X
10	$\rho^3 \cos(3\theta)$	Trefoil 0°
11	$\rho^4 \sin(4\theta)$	Tetrafoil 22.5°
12	$(4\rho^4 - 3\rho^2) \sin(2\theta)$	Astigmatism 2nd order 45°
13	$6\rho^4 - 2\rho^2 - 1$	Spherical
14	$(4\rho^4 - 3\rho^2) \cos(2\theta)$	Astigmatism 2nd order 0°
15	$\rho^4 \cos(4\theta)$	Tetrafoil 0°

These polynomials are generated by laser interferometers that using sophisticated computer algorithms examines the surface figure of the substrate, and converts that data into the Zernikes to be interpreted.[34] The polynomials will then be sued to categorize the figure profiles on the particular surface of the optical component that is being tested. For example, when evaluating planer optics, the appearance of a sixth order astigmatic surface profiles on a surface is a sign of improper weighting when using the pitch polish process. Either the amount of weight needs to be changed, or repositioned in order to have a more randomized surface profile rather than a concentric annulus forming on the surface.

3. Materials and Methods

The overall project is separated into four primary segments, design, manufacturing, and

[34] Goodwin, E. P., & Wyant, J. C. (2006). *Field Guide to Interferometric Optical Testing*. SPIE Press.

assembly, and testing. Each one requires a unique skill set and background knowledge to produce the highest quality opto-mechanical assemblies. In addition, a separate mechanical design for a large tilt-stage is also included which is used during the testing process for this optic.

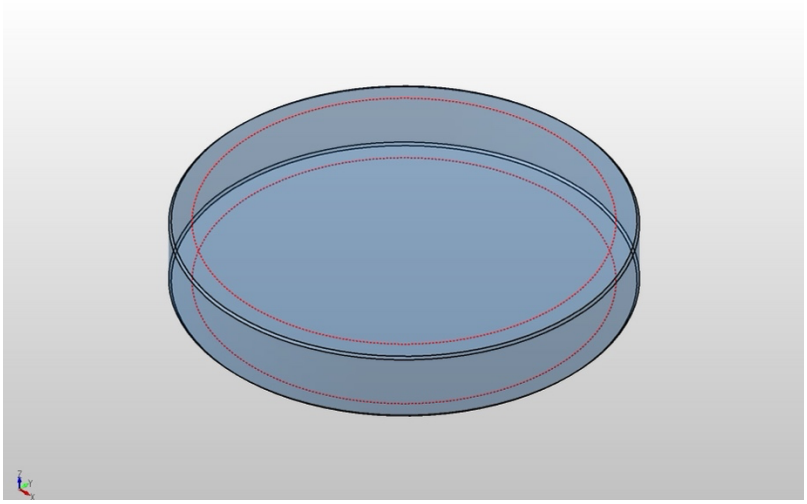

Figure 9. 3D CAD model of 330mm Diameter by 50.8mm Fused Silica Transmission. This is standard size and material for transmission flats used by metrology equipment OEMs.

Table 3. Customer Requirements for Assembly 330mm Transmission Flat

Type: Round Diameter Flat
Material: Corning 7980 0A HPFS
Diameter: 330.00mm ± 0.25mm
Thick Edge: 50.8mm ± 0.25mm
Wedge (across diameter): 0.2 Degrees ± 0.1 Degree
Clear Aperture: 90% of Central Diameter
Surface Quality: 40-20 Per MIL-PRF-13830B
Surface Flatness (S1 & S2): λ/10 PV at 632.8nm

Surface Roughness: Less than 10 Angstroms
Coatings: Anti-Reflective Coating on S2 at 632.8nm, Normal AOI, R < 0.5%

The customer, whom we have been told has acquired a 12-inch beam-expander that will be matted to a Zygo GPI Interferometer, provided the mechanical specifications of the flat (See Table 1). The 330mm diameter was chosen, as it would provide the adequate aperture size for their applications (See Fig. 9). Manufacturing approaches were taken that would optimize the manufacture of the flat to meet the customer specifications.

Although it can be difficult at times to identify the best approach for certain optical components, for high precision substrates such as reference quality optics that we are discussing, the tradition grinding and polishing method is the most ideal approach to approach this challenge.

The grinding and polishing method uses an approach that slowly removes a smaller and smaller amount of material over a long determinative process. With single sized grinding and polishing, parts are placed on a precision grinder or polisher, sitting down on the surface by gravity during

the lapping process. The rotating lapping process have cutting fluid/polishing compound that is used in conjunction with the grooves on the surface that slowly removes materials from the bottom of the substrate. Precision fixtures and handling is key for both achieving the desired specifications, but also for the safety of the part, since much of the handling is done by hand. Part of this is due to the fact that parts need to be taken on and off the polishing equipment, in this case with single-sided pitch polishing, they are removed by hand (or with suction cups if the substrate is too heavy), and then transferred onto a cart to move between operations. For the drawback in terms of the slower pace of fabrication, the tradeoff is that the customer gets superior quality optical components compared with other methods.

These special considerations are then integrated into the overall process design of the fabrication approach and were made to ensure that the specifications provided by the customer were met. The manufacturing process is relatively the same at other manufacturing facilities that produce high precision substrates, the real innovated processes are unique to every company, and Precision Optical's ability to produce high quality optics is mainly due to the skill and experience of the optician who work on the manufacturing floor.

3.1 Design of the Opto-mechanical Mount and Large Component Tilt Stage

The most design engineering intensive part of the process is the mechanical design of the housing that the substrate will be mounted on. The following is a list of some of the major design consideration that needed to be considered.

The novelty of this approach is that rather than using an adhesive based model, which is more commonplace, this takes a different approach to securing the flat using a non-adhesive method, which allows for ease of dis-assembly and repair of the substrate if needed. Other considerations are that the chances of there being any outgassing from adhesives, which range from RTVs to

structural epoxies, which could limit the environments that interferometric systems are able to be used.

In addition, as will be described below, the use of compression springs to engage the load is a novel approach to what is currently being offered on the market. This approach not only holds the substrate in the correct position to ensure that the clear aperture is within the field of view, but also distributes the weight more evenly across the lower end of the flat, which creates a more randomized and uniform stress profile as shown in interferometric testing.

3.1.1 Design of the Mount:

The assembly needed to be able to fit the 330mm TF, and provide a large enough opening in order to encompass the clear aperture. The octagonal design was chosen as it provides segmented 45-degree clocked segments that provide locations for mounting handles and provides a stable segment for the assemble to rest on.

Another design consideration is ergonomics, as handling and transporting the flat is important to take into consideration (See Fig. 10). Again, the octagonal main structure of the assembly allows handles to be mounted on the top part of the assembly. This makes it comfortable to transport and to mount on the beam expander. In addition, the mount is symmetrical from back to front, just in the case the flat was assembled in the wrong orientation (AR Coated Side at the ‘front’), the mount and be reversed and placed on in reverse.

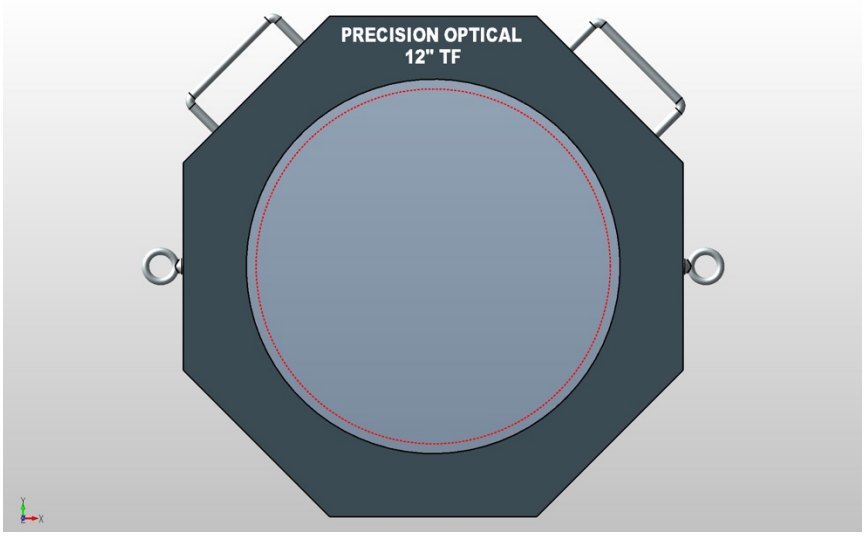

Figure 10: Fully Assembled Transmission Flat into Mount. The Mount is made out of 6061 T6 Aluminum, and is used hold the flat in place I which the optical axis of the collimating lens will line up with the primary optical-axis of the main flat.

The flat is being secured by a combination of vibration absorbing rubber, and mounting pads placed (rotationally clockwise) at 0 degrees, 135 degrees, and 215 degrees. These are the primary structures that will secure the flat to the assembly. An adhesive option was considered, and is used standard to secure flats to mounts on many beam-expanded TFs. The front and back plates has also been hard anodized the color black as to reduce the chance of stray light reflecting off of the assembly, which could have adverse effects on the measurements. Also, the vibration absorbing rubber has the pliability to compensate for the wedge that is put on the backside of the flat, while still distributing the even pressure.

However this design is different as it was designed to be able to mount the flat into the mount without adhesive. This was chosen (sans adhesive) as it places compression force on the flat, rather than tension being pulled on from adhesive. This is commonly seen when observing mounted flats that are being secured by adhesive into their mount (which is then mounted to a

mating section on the interferometer). See example below from a 4.000” Aperture TF after assembly bonded with Dow-Corning 733 glass to metal adhesive into an aluminum cell (See Fig. 11). Even though the flatness of the surface is very impressive (0.017 waves PV at 632.8nm), the locations of pull from the adhesive are still visible on the interferogram. Although this has not shown to cause any major issues with the measurement accuracy, as it is standard practice for securing flats. This new assembly is attempting a different approach that will put distributed pressure rather than a pull as seen in the assembly below.

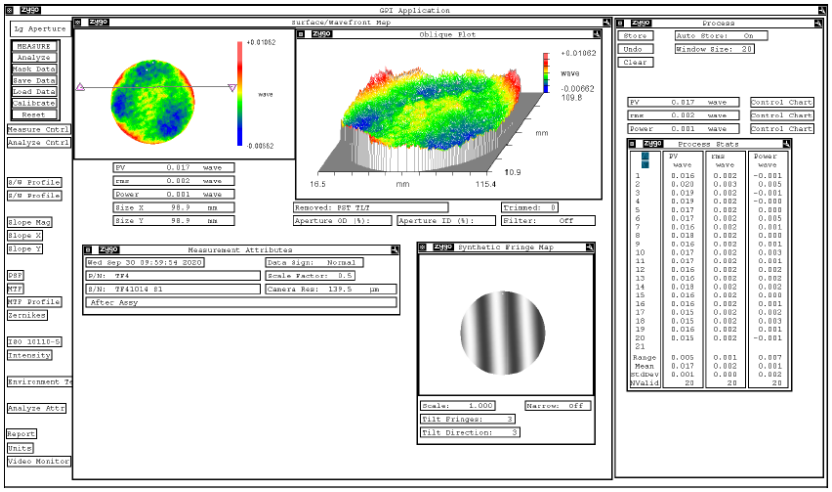

Figure 11. Interferometric Data from Zygo ATZ with a 480mm Beam Expander depicting the transmission flat prior to assembly. Here, the transmitted wavefront error is being measured at 0.017 waves peak to valley at 632.8nm after it has been assembled with a low outgassing adhesive into an aluminum cell.

The first part is accomplished using vibration-absorbing rubber strips (in red) that are distributed around the front and back plate of the assembly (the pads are also on the mounting pads (See Fig. 12). The pads are evenly distributed around both the front and back plate of the assembly. This provides light pressure (designed to have < 0.25mm of compression), while being supported by

the pad. The main purposes of the rubber strips are to hold the TF secure while being seated vertically.

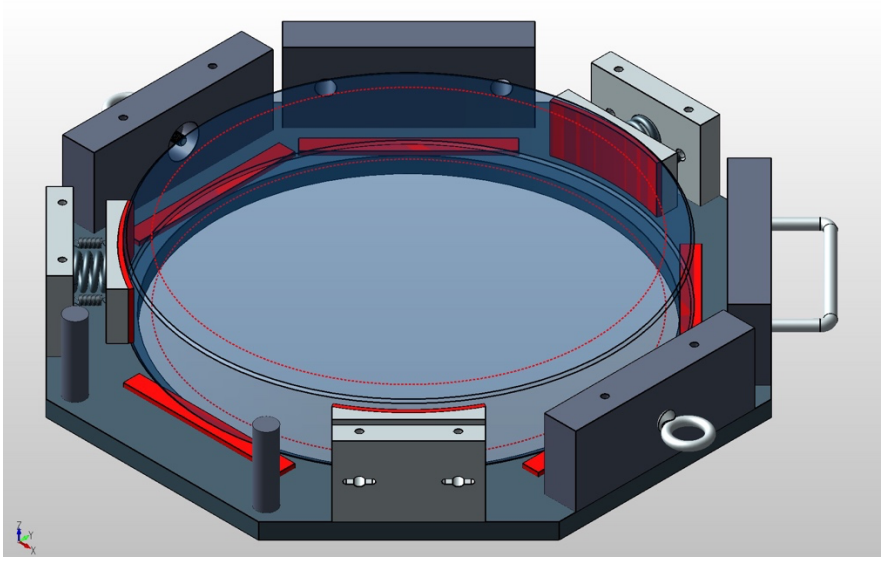

Figure 12. 3D CAD drawing showing the transmission flat laying inside the mount housing prior to the front cover being assembled. The substrate is laying down on 10 vibration absorbing pads (five on each side of the housing) in order to stabilize the flat.

The main securing apparatus that supports the force due to gravity are the mounting pad as seen in the images below. The pads are made of aluminum, and the top portion is also lined with the vibration resistant rubber, and machined with a radius of curvature that matches that of the substrate. In addition to the rubber pads, a compression spring is used to absorb the force due to gravity from the flat, approx. 9.5kg. Extension springs are added and secured with dowel pins to hold the mount assembly together (See Fig. 13). The lower mounted compression springs along with the rubber lined top plate will cradle the flat, and will distribute the force between the two pads equally (See Fig. 14). The top-mounting pad is used to provide additional support, and is designed to imping minimal amount of force in the y-direction.

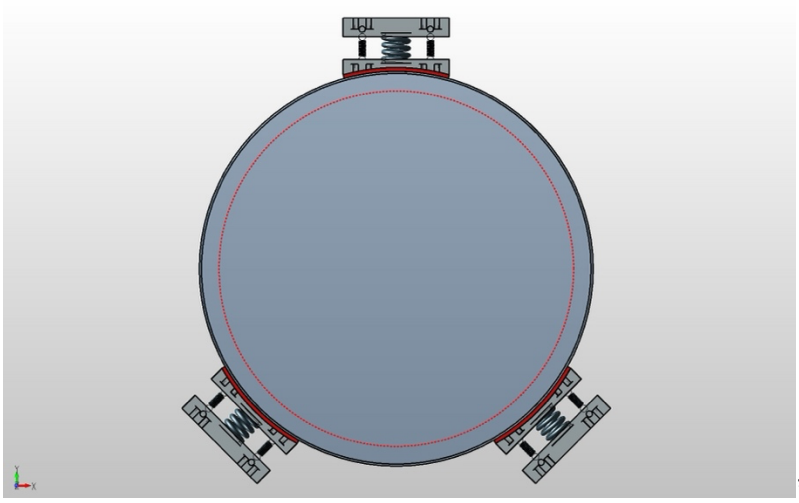

Figure 13. Image of the 330mm transmission flat being supported by three engagement pads in free space. Note that the surface engagement pads are supporting the weight with both the assistance of the rubber engagement pads as well as compression springs (K = 415lbs/inch).

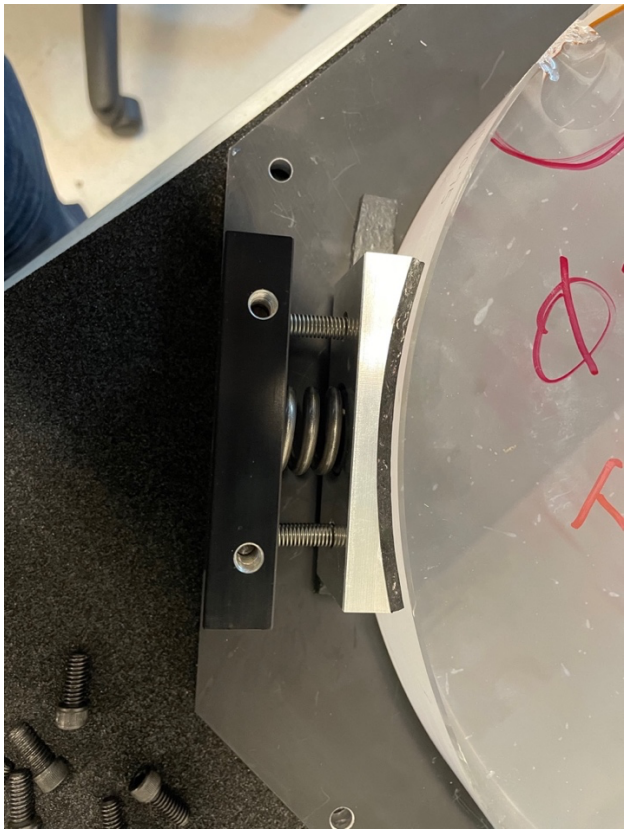

Figure 14. Zoomed in image of engagement pad making contact with testing fused silica flat. The radius of curvature of the engagement pad is matched to that of the outer diameter of the substrate. The vibration resistant rubber pads are adhered to the metal component using a low outgassing adhesive.

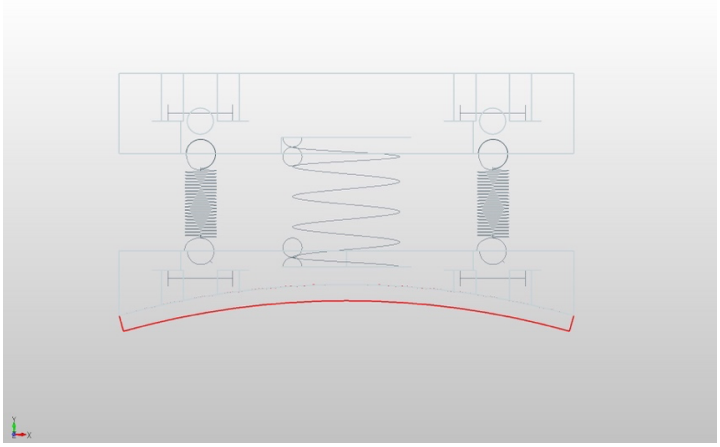

Figure 15. CAD design of engagement pad. The springs were purchased as standard products from McMasterCarr.

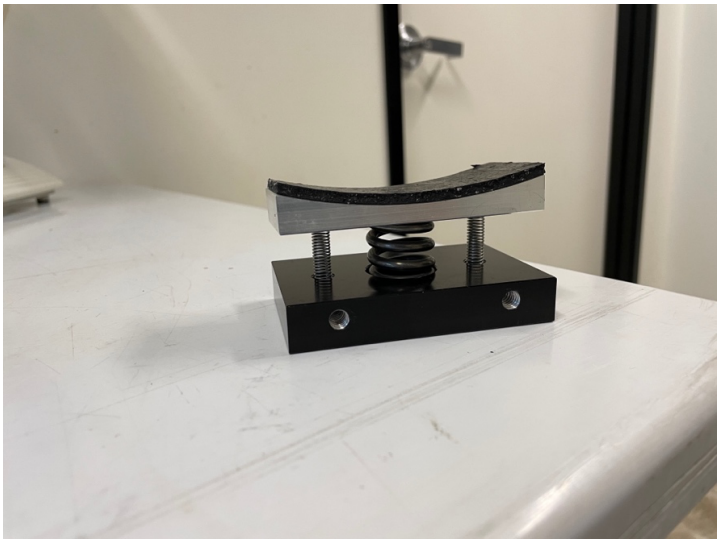

Figure 16: Fully assembled engagement pad.

As a horizontally mounted optic, and based on the intended design and use case of the mount, an analysis must be performed to determine the loads, forces, and relative stiffness of the

components[35]. The primary goal of this analysis is to determine the survival, performance, and RMS uncertainty in the measurement results of the transmission flat. The overall goals are:

1. Now having the stiffness, what are the perturbation forces in the environment
2. Can the amount of RMS measurement error be estimated from the environment?

An analysis was performed to determine on the stiffness under deflection of the pads, specifically the two lower pads that are bearing the brunt of the load of the substrate's downward force due to gravity (See Fig. 17) as experienced as load on the spring assembly (See Fig. 18).

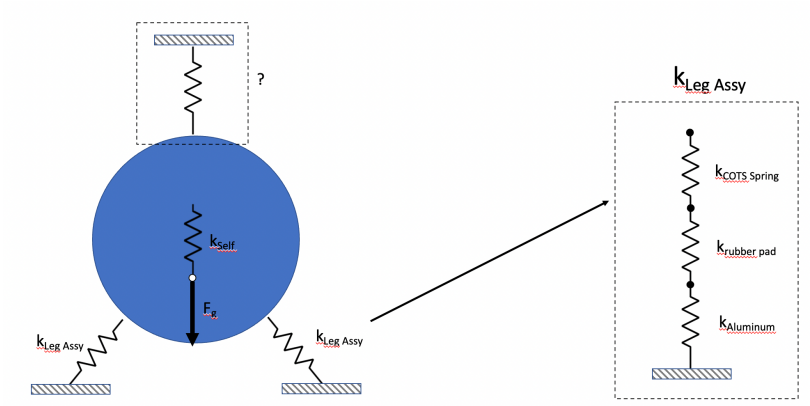

Figure 17. Freebody diagram of two optics on two – point support, normal horizontal loading.

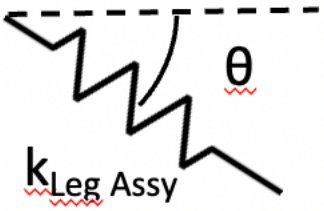

Figure 18. Two component horizontally loaded spring.

$$k_{Leg\ Assy\ Horizontal} = k_{Leg\ Assy} cos^2\theta \tag{29}$$

[35] Yoder, P. (2015). In D. Vukobratovich (Ed.), *Opto-Mechanical Systems Design DESIGN AND ANALYSIS OF LARGE MIRRORS AND STRUCTURES* (4th ed., Vol. 2, pp. 121–122). essay, CRC Press.

$$k_{Leg\ Assy\ Verticle} = k_{Leg\ Assy} sin^2\theta \tag{30}$$

The resulting calculations using (Eq. 9), (Eq. 29), and (Eq. 30) (see Appendix A.) would result in a first-order stiffness under deflection load of 25863.47 N/µm. This result show that the stiffness of the optic is so high that it does not need to be taken into account when it comes to any deformation, such as the shape of the clear aperture moving from a theoretically perfect circle to an ellipsoid geometry.

When analyzing the rubber pad assembly, the resulting calculations demonstrated a similar result, that the stiffness is so high that the force needed to create a displacement is negligible for the calculation.

Another important consideration is if the displacement due to gravity would result in the optical axis and/or clear aperture to have shifted from the free aperture of the mount (See Fig. 19).

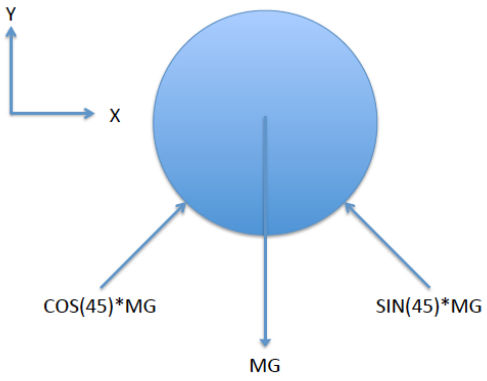

Figure 19. A free-body diagram of the substrate being supporting by the two engagement pads, and the displacement induced by gravity and dampened by the compression springs and vibration resistant rubber pads.

$$Volume_{TF} = \left(\left(\frac{33cm}{2}\right)^2 \times \pi\right) \times 5.08cm = 4{,}344.917\ cm^3 \tag{31}$$

$$Density_{Fused\ Silica} = 2.204\ \frac{grams}{cm^3} \tag{32}$$

$$Mass_{TF} = Volume_{TF} \times Density_{Fused\ Silica} \tag{33}$$

$$Mass_{TF} = 4{,}344.917 \times 2.204 = 9{,}576.197\ grams \tag{34}$$

$$Force_{TF} = Mass_{TF} \times Acceleration_{Gravity} \tag{35}$$

$$Force_{TF} = 9.576\ kg \times 9.8\ \frac{meters}{seconds^2} = 93.847\ Newtons \tag{36}$$

$$\Delta L_{Gravity} = \frac{\cos(45) \times Force_{TF}}{K_{Spring}} = \frac{\cos(45) \times 93.847\ Newtons}{73728.346\ \frac{Newtons}{Meter}} = 0.68mm \tag{37}$$

Performing an analysis using Newtonian mechanics, it was determined that the displacement due to gravity (when accounting for the spring constant) would be approx. 0.68mm (Eq. 37). This is essentially negligible and would have no effect on the centering of the optical axis.

The pads themselves are made out of aluminum, which is both durable enough to support the apparatus as well as light enough so when combined with the flat, it is still possible to carry the who assembly by hand. In addition, the forces generated from other items such as the extension springs and the force due to gravity from other components of the mount are negligible compared to the force from gravity of the flat, and would not contribute significantly to the displacement of the spring, and thus were not added to the calculation.

Next, an analysis into the natural frequency of the spring assembly was performed to see if there needs to be any additional damping in the system. Using (Eq. 25), the natural frequency of our system simplifies into:

$$f = \frac{\sqrt{\frac{73728.346}{93.847}}}{2 \times 3.141} = 4.462\ Hz \tag{38}$$

This results a 4.462 Hz natural frequency for this system (Eq. 39). The assembly and the equipment that was used to do the interferometric testing was done on a Newport Active Dampening Air Table. The horizonal isolation was rated to be 80% at 5hz, and the vertical isolation was rated to be 86% at 5hz[36]. Based on the calculation of the natural frequency of our system being around that value, we felt comfortable stating the any vibration have been damped and/or have been negligible.

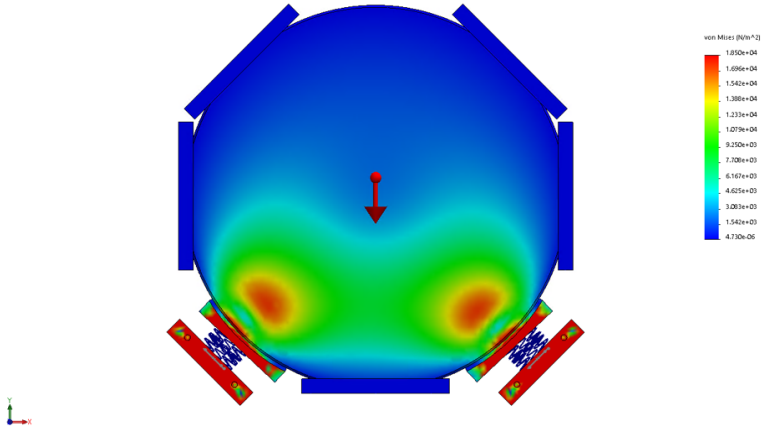

Figure 20: FEA Analysis, Von Mise Analysis of the 330mm Transmission Flat Mounted into the Adhesive free mount.

Finally, an FEA analysis was performed using SolidWorks®, and materials were assigned, and the spring constant *k* was applied to the springs. The extension springs provided negligible force, as their main purpose is to hold the engagement pad assembly together, and thus their spring constants were not added to the model.

Looking at the results of the FEA von Mises analysis (See Fig. 20), the primary sources of stress with respect to gravity, as expected is located at the surface contract points of the engagement

[36] *Optical table system, ST-UT2 smarttable®, 5 ft. X 10 ft., 12 in. thick*. OTS-UT2-510-12-I Optical Table System. (n.d.). Retrieved August 14, 2022, from https://www.newport.com/p/OTS-UT2-510-12-I

pads and the substrate. From both the FEA and the earlier first-order analysis, the loads are at least 3 magnitudes away from failure. The elastic limit according to the material OEM, Corning, is between 152.2 to 167.8 MPa[37]. So, when observing the data from the FEA analysis, the max pressure in the model at 1.611 KPa, there are no stress concentrations to worry about as they are negligible in magnitude compared to the limit needed to achieve failure.

Another consideration is that glass, specifically in this case fused silica, is a relatively brittle material. A material is considered brittle when it fractures with little elastic deformation when subjected to a force. In this case, a FEA analysis may not be the ideal form to assess the failure potential of glass. Large compressive stresses would result in large von Mises stress, but wouldn't cause any flaws or cracks to propagate in the material (which is most often the cause of failure). A failure criterion based on the first principal stress is more commonly used for brittle materials.

3.1.2 Design of the Tilt Stage

In addition to the mount for the flat, a tilt stage was also designed for the customer. Stages such as these are needed in order to assist in nulling fringes during the data acquisition process when performing interferometric metrology. For smaller components, similar tip-tilt stages are used to perform the same operation.

The tilt-mechanism is a combination of ball-bearings press-fit into bearing housings which are screwed down into the bottom plate. The bearings and the top plate are connected with a shaft that is connected to the top plate. The plates are held down using a combination of four spring

[37] *High purity fused silica: HPFS fused silica*. Corning. (n.d.). Retrieved August 14, 2022, from https://www.corning.com/worldwide/en/products/advanced-optics/product-materials/semiconductor-laser-optic-components/high-purity-fused-silica.html

screws with spring washers, and a center screw that is used to adjust the maximum amount of tilt that is allowable. The components were machined out of aluminum, and additional components were purchased from McMasterCarr and are made out of steel.

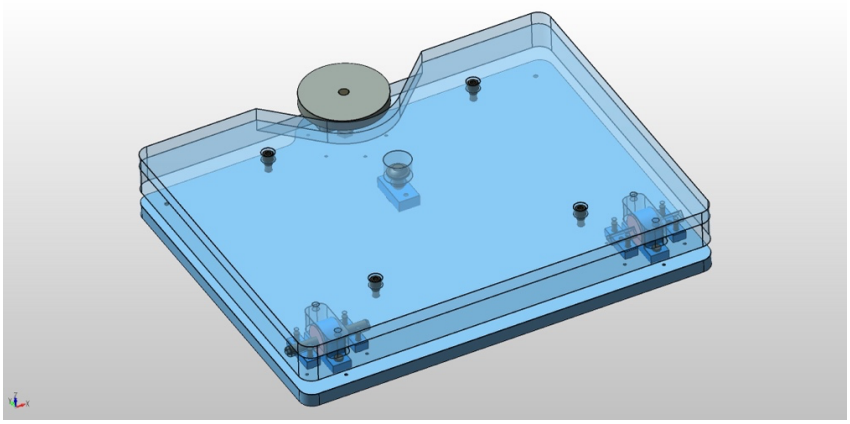

Figure 21: Large Tip Tilt Mount, CAD Model, Isometric View

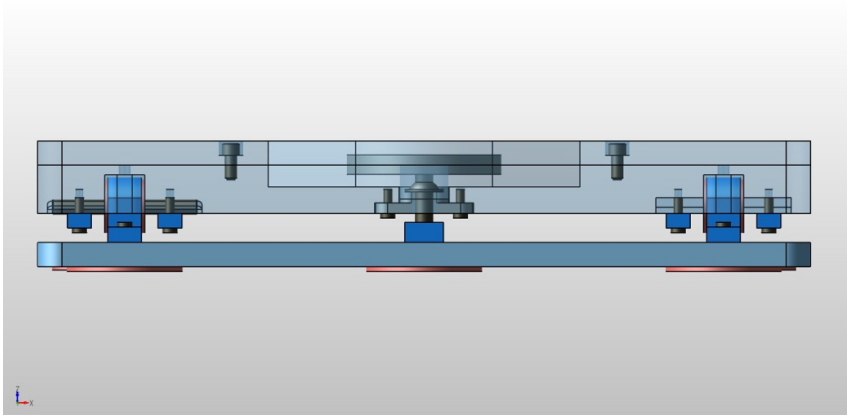

Figure 22: Profile View

The tilt stage will be placed on a metal air table. The feet were designed to have Teflon coated pads on the bottom to provide ease of travel on the table. The bottom of the plate has a three-feet kinematic design to prevent any rocking that may occur and disrupt measurements (See Fig. 22).

The main adjustment knob was matted with a high travel screw from MKS Newport Corp. to

provide a fine level of adjustment for the tilt mechanism.

The large tilt stage has a footprint of 14.000” X 16.000” X 2.600”. The dimensions were designed to accommodate the sizes of components that the customer plans on supporting to use along with the TF assembly (See Fig. 21). The height was designed so that the top plate of the stage will be 1.000” below the TF assembly. The stage was designed to only have a tilt feature, as other Euler rotations can be performed on the part itself, thus only a single axis needs to be constrained.

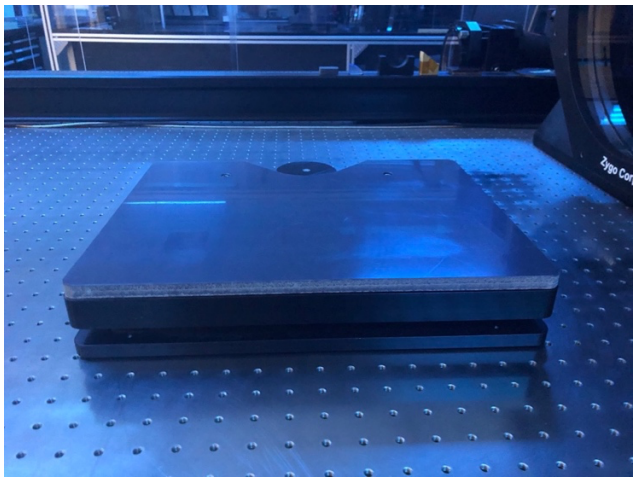

Figure 23: Large Tip-Tilt Stage, Complete and Assembled in profile view

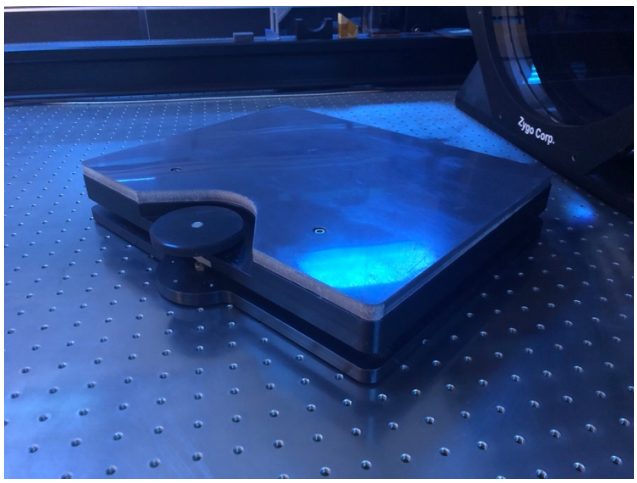

Figure 24: Isometric view of Large Tip-Tilt Stage in isometric view.

The top and bottom plates of the stage were hard anodized black, as to reduce the chance of stray light reflections coming off the stage that could disrupt the measurement, such as causing difficulty aligning the part (See Fig. 23). The top plate of the stage has also been covered with a Teflon film used both as to protect the part from direct contact with metal, as well as provide an easy cleaning surface that can be cleaned with acetone or methanol (See Fig. 24). If the film becomes damage due to physical abuse caused by placing and removing large substrates on it, then it can also be replaced fairly easily.

3.2 Design of the Manufacturing Process

The traditional grind and polish fabrication process for high precision reference quality substrates had been developed over many years, and are ever improving due to the availability of higher resolution metrology instrumentation. When selecting a fabrication approach, there are a number of items that has to be considered.

Selection of Material

For high precision reference quality optics, the selection of a stable, high homogeneity material is key to providing reliable data from your instruments. For most interferometric applications, reference optics made out of a high purity fused silica is the most common choice, due to its stability and high homogeneity. Index Homogeneity is a specification that refers to the maximum amount of index variation over the clear aperture of the substrate. For this particular application, Corning© 7980 was chosen as the material type. At the request of the customer, A grade material was chosen, which is the second highest grade of fused silica available by Corning, and a bubble and inclusion grade of 0. A low bubble and inclusion count is important because a large number of defects has the potential to harm the transmission quality of the optic.

Stress Relief

During the machining process to fabricate the initial raw substrate (in this case a 330mm Diameter by 50.8mm in Thickness), subsurface damage is induced which can have a negative effect on the transmission quality of the substrate. Therefore, a multi-stage grinding process is commonly used in order to relieve stress from the surfaces to be polished. This is done by grinding off material using multiple loose-grit sizes, taking off at least 3X material relative to the size of the loose grit. This is done on a continuous grinder, which rotates a cast iron grinding surface about a center axis while the substrate is fixed in place. For this particular application, a three-stage grinding process was used. First a vertical rotary grinder (or Blanchard mill) using a 220-grit wheel to remove material and apply a 12-arc minute (0.2 degrees) wedge into the back (non-reference) surface of the substrate. This wedge was applied to prevent light from being reflected back into the interferometer after its aligned. After, a two stages operation on the continuous grinder is commenced. First with a 15-micron grit loose abrasive, and then with a 9-micron grit loose abrasive. In total, approx. 0.5mm of material was removed from each surface prior to polishing. In addition, it is not unheard of for customers to request that the outer barrels and chamfers of the substrate be polished as well in order to achieve additional stress relief. However, this particular customer did not request this.

Coatings

For all precision optical components to function, a thin-film coating deposited in a vacuum chamber in order to provide better reflectivity or better transmissibility (or in the case of beam-splitters some percentage of both). Often times, an anti-reflective coating is applied to the back (non-reference) wedged surface of the substrate. The front (reference) surface is typically uncoated, or has an attenuator coating on it to reduce the amount of light transmission that is getting through. This back surface is usually oriented at the back of the mount. An anti-reflective

coating is typical for these types of components, was applied to this particular substrate. The decision to add the anti-reflective coating was done at the request of the customer.

Following the design of the components and the respective equipment, an assembly process was developed to provide a clear and understandable approach to mounting the TF into the mount. This procedure describes how to mount the standard (non-flexure mounted) T-Flat or R-Flat in its assembly in the proper orientation and rotation. Specific assembly adjustments and other skill-sensitive functions will be determined by the optical assembler's experience and/or the supervisor's guidance. All functions referenced herein are well known in the optical manufacturing field and the instructions will be delineated to the degree of detail necessary for understanding by an experienced optical technologist or optician.

Data was collected throughout the manufacturing process, with in-process metrology being performed during the polishing stage by technicians. The raw material substrate was ordered from Corning Specialty Materials in New York, and was polished on a single sided pitch-polishing lap.

The substrates were determined to use Precision Optical's tried and true process for the production of high precision optical components. This process has been used often for manufacturing round optical components that are 300mm and greater.

The substrates first begin in the shaping department, in which subsurface damage from the substrate OEM is removed by milling off approx. 0.1mm to 0.2mm of material from both surfaces. In addition, a 0.2 degreed wedge across the diameter of the substrate is applied, that prevents light being reflected directly into the instrument when installed. The vertical rotary grinders (or Blanchard Mills known colloquially), using a 180-grit fix grit diamond grinding

wheel. This also brings the part into its near-net dimensions, approx. 0.1mm above the top of the tolerance of the thick edge dimensions.

Figure 25: Initial Shaping Process of flat to remove subsurface damage using Blanchard Mill with 180 Grit Wheel.

Following the Blanchard operation and the subsequent cleaning and quality assurance, the parts then go through a multi-stage grinding operation to further reduce any subsurface damage, and to achieve final mechanical dimensions (See Fig. 25). The removal will be done in multiple stages using multiple grit sizes. The top of the laps themselves is made out of cast iron, and rotates about its central axis (See Table 4). The removal amounts are as follows (both sides):

Table 4. Multi-Stage Grinding Layout

Operation	**Grit Size**	**Removal Amount**
Shaping (both sides)	180 Grit	0.1mm – 0.2mm
Grinding (both sides)	15 Microns	0.1mm
Grinding (both sides)	9 Microns	0.1mm

Figure 26: Grinding Laps being prepared to grind substrate with 15 Micron Grit

The rule of thumb for remove amount is to take off a minimum 3X the amount of material as the previous grit size, which is an industry standard used by organizations such as NASA's Jet Propulsion Laboratory and defense contractors. For high precision applications, this process is standard for Precision Optical when it comes to grinding process.

The cast iron grinding tops are cut with groves that will remove material from the substrate. An Aluminum-Oxide grinding compound is used as a lubricant for the grinding operation (See Fig. 26). The parts are then placed down onto the grinding tops (on the surface to be worked on), and then weighted on the opposite side while the grinding top rotates to remove material.

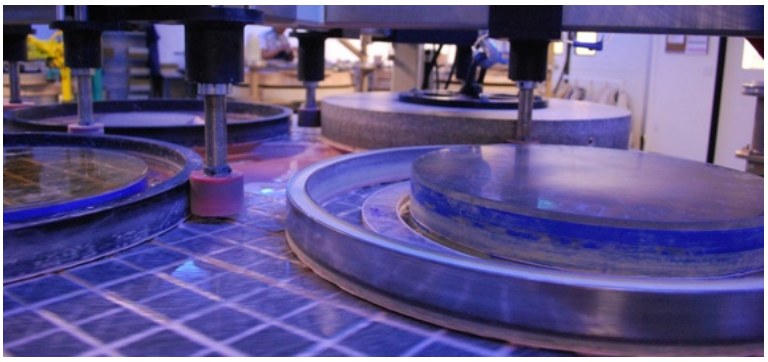

Figure 27: Substrate on Polishing Lap for final angular correction and surface figure production

Figure 28: Precision Optical Polishing Department with single sided pitch polishing laps

The pitch is comprised of a proprietary compound, with similar properties to tar (See Fig. 27). The polishing solution is a 0.5-micron loose grit cerium-oxide based solution, which breaks down into < 0.25-micron sizes over time. This is diluted with distilled water during the polishing operation. Although many processes have been automated, optical polishing is still regarded as more of an art form rather than an exact science, meaning the parts are manufactured deterministically, with regular in-process metrology being performed until it reaches its desired specifications, rather than implementing an exact formula consisting of rotation speed, dilution, time, and weight, that would reliably produce the desired outcome.

The pitch polishing laps are operated by technicians that have on average 25 years of optical fabrication experience. The lap rotates in a counterclockwise motion, with groove cut in by hand (determined by the preference of the technician), and varies from 30 inches in diameter to 84 inches in diameter. The polishing lap that this 330mm flat was polished on a 76-inch polishing lap (See Fig. 28). The part is encompassed in a polishing ring that is approx. 30% larger in diameter than the part itself. The main purpose of the ring is to prevent the substrate from falling off the polishing lap, but also provides a bumper that rotates the part in a randomized motion. This randomized motion prevents any annulus regions for developing, which reduced the need

for generating a subtracting file that matches the surface figure of the flat that needs to be applied while being used as a reference surface.

Table 5: Consideration Prior to Assembly

Verify that Flat has been inspected and found to pass surface quality (scratch/dig) specifications prior to beginning this procedure.
Flat mounting must be performed in the Assembly Lab at nominally 70.0°±3.0°F at start of mounting process.
Set Assembly Lab temperature and wait for room to stabilize.
Verify temperature reading in the lab is within parameters described above.
Once lab temp is stable, record nominal starting lab temp on data sheet.
Circle on data sheet the type of flat to be mounted: T-Flat or R-Flat.

When mounting an optic, there are a number of considerations take into account, and to ensure that the tolerances are within range (See Table 5). There is a delicate balance between the optic fitting too tightly, which can induce stress to the substrate as well as increase the risk of fracturing the optic. The stress induce could potentially change the surface figure of the optic,

which in turn adds potential error to the measurements. This needs to be taken into consideration when examining the tolerances of specifications such as outer diameter, center thickness, wedge, chamfers, and roughness of the edge barrel.

Another consideration is the environment that the mounted optic will be inhabiting. In a lab environment with standard temperature and pressure, the need to take in co-efficient of thermal expansion (CTE) is not a major concern. However, if the assembly is going to be exposed to changes in temperature such as a camera lens pack mounted externally on the outside of an automobile, then CTE considerations needs to be taken into account.

3.3 Designing the Testing Process

The testing process for reference quality optics generally follow the same procedures as would other large optical components. However, a key consideration is that since these optics will be used to assess the quality of other optics, the level of precision and the amount of documentation that is needed is greatly scrutinized. For example, many reference quality optics are required to ship with the final interferograms, as well as a certification from the fabrication and/or testing facility. In addition to interferograms, an inspection sheet with the mechanical dimensions, as well as a surface quality map is also included with the final shipped part. This data is useful not only for the user to better integrate the reference optic in the system, but it also provides useful data in the event that the substrate will need further repair down the road from wear and tear.

3.3.1 Pre-Assembly

The main premise of a Fizeau interferometer is measure the surface height differences between two surfaces. In both cases, the pre and post assembly process, the substrate was left to acclimate in the enclosed acrylic chamber inside on the air table. This is standard procedure, especially for high precision substrates such as reference quality optics (See Fig. 29). The polishing and

assembly processes has the potential to induce heat into the material, as it is moving on the pitch polishing lap or being adjusted during the assembly process.

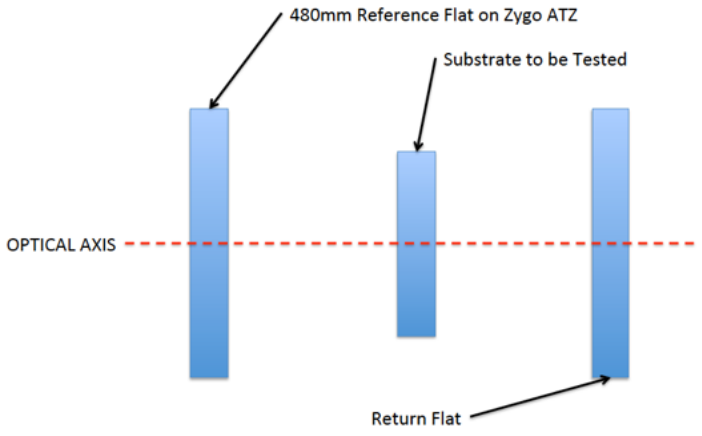

Figure 29: Testing Layout of ZYGO Interferometer of Pre-Assembled Substrate

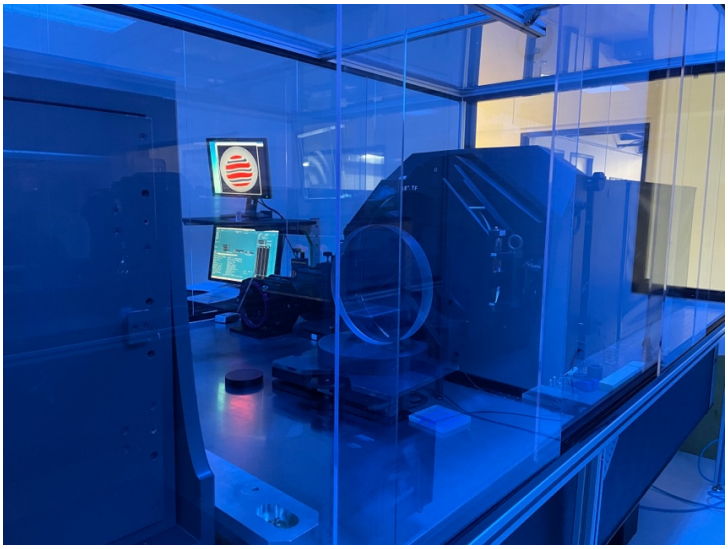

Figure 30: Substrate in-front of ZYGO Interferometer being tested for surface figure, on the Newport Active Dampening Air Table inside an acrylic closure

The flat was left to acclimate prior to the measurements for approx. 12 hours in the enclosed environment (See Fig 30).

Following the post metrology process, the part went into coating, where an anti-reflective coating will be applied to the backside (S2) of the flat. Depending on the application, it is not uncommon to put an attenuator coating on the front side to reduce the amount of light, and mitigating saturation into the instrument for better data results.

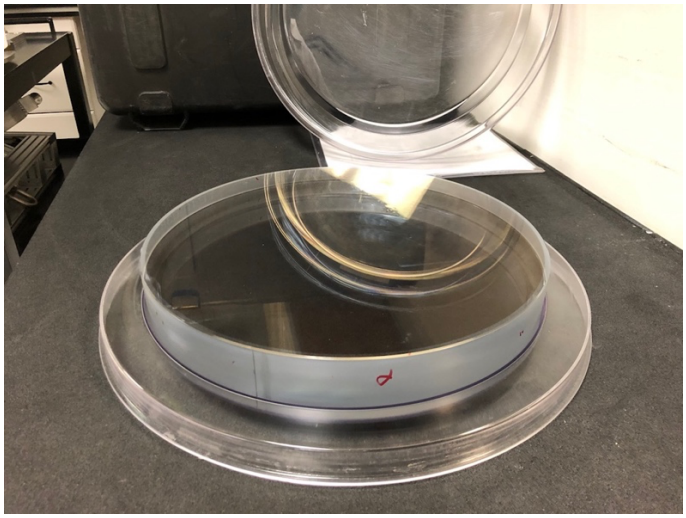

Figure 31: 330mm Transmission Flat Finished Substrate Pre-Assembled Secured in PET Package for transport around shop environment

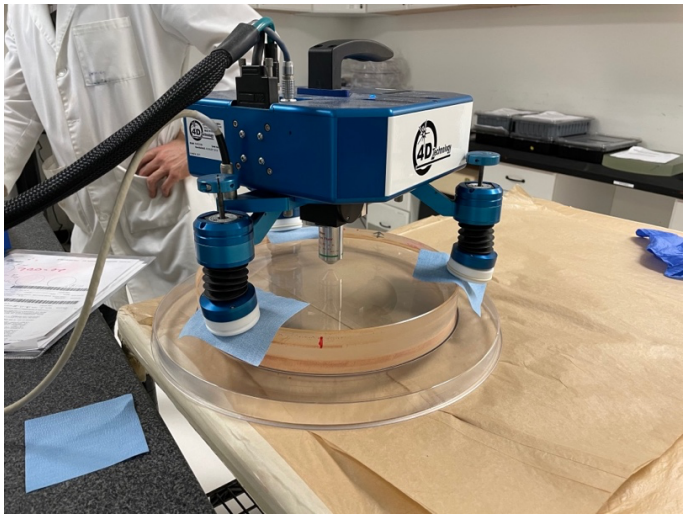

Figure 32: Flat being tested using surface profilometer for surface roughness.

The flat was transported during the fabrication process using a custom designed PET-G package (See Fig. 31). The package held the flat by its chamfers, and thus the polished surfaces are protected from any potential defects.

A surface profilometer, in this case the NanoCam manufactured by Tucson based 4D Technology, was used to assess the surface roughness of the optical surfaces. Low surface roughness prevents minimizes the scattering of stray light (See Fig. 32). Because the roughness specification is much smaller than a wavelength of light (approx. three to five angstroms), the likelihood of ghost imaging in the system is small.

3.3.2 Post-Assembly

Post assembly, the surface figure shows that the distributed pressure around the flat produced a more evenly distributed than compared to the flat with the one with the adhesive bonds. Although this is not a representative comparison (i.e., the adhesive bonded flat is much smaller), it would not be unreasonable to assume that a similar approach would produce a similar interferometric data.

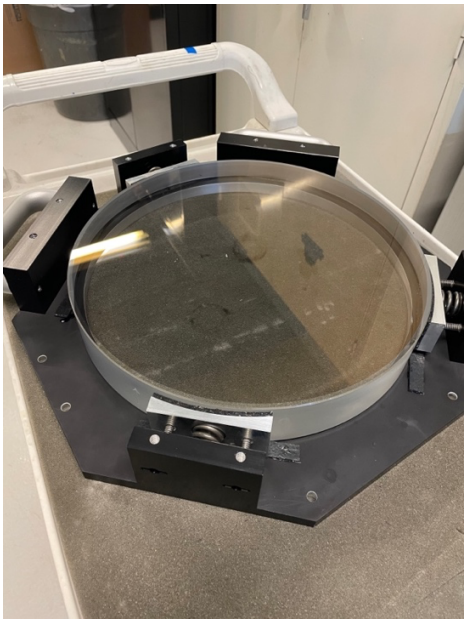

Figure 33: 330mm Transmission Flat Substrate being assembled into mount, engagement pads are being assembled to the outer barrel of the substrate

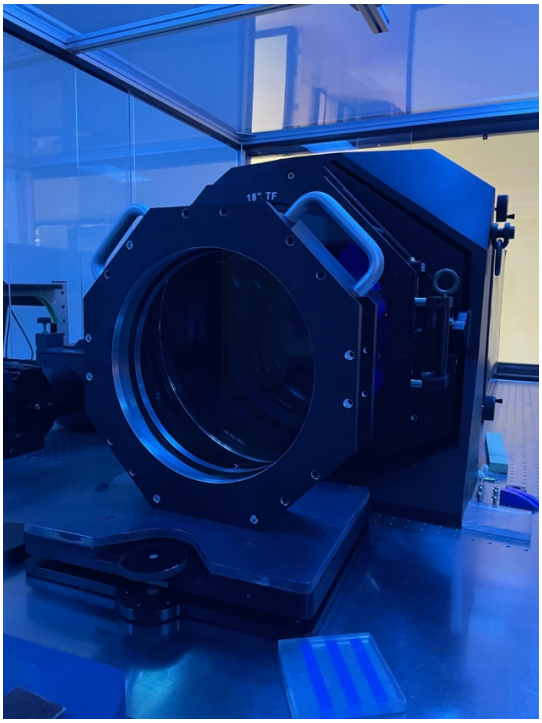

Figure 34: Fully Assembled substrate with mount being tested on for Surface Figure on ZYGO Interferometer

The flat was assembled into the mount by hand since this is a delicate operation (See Fig. 33). The flat was carefully laid down on the vibration resistant pads that were already adhered to the backside of the back plate. After the flat was laid down on top of the pads, the engagement pads were then fixed around the perimeter. Then, the handle block and the mounting block were assembled onto the flat. Finally, the top plate was then affixed to the top of the mount, and the whole assembly was raised vertically.

The mount was then measured on the interferometer in the same configuration as with the pre-assembly flat using the full aperture of the 18” beam expanded Zygo ATZ (See Fig. 34). The

whole assembly was left to acclimate to the environment for approx. 12 hours prior to taking the measurements.

4. Results

A set of interferometric data was collected both pre and post assembly in order to assess the performance the transmission flat, and to assess how much the addition of the mount affected the surface figure data of the substrate (See Fig. 35). The after a set of 20 measurements, each of which takes approx. 10 seconds to perform, the data is then averaged to result in a single surface figure number.

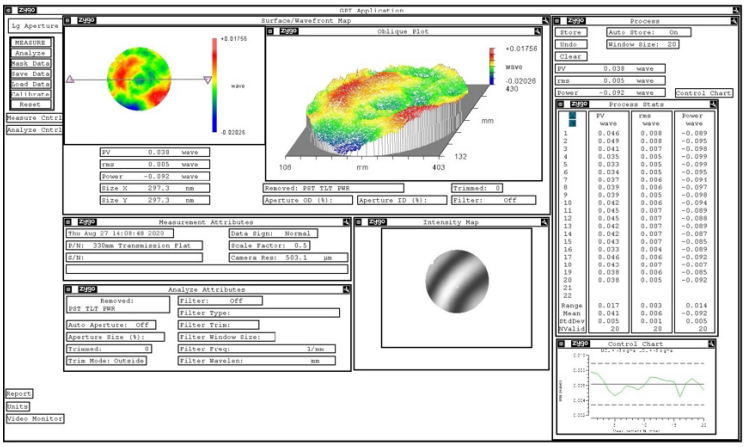

Figure 35: Interferogram of Transmitted Wavefront Error of unassembled substrate at 0.036 waves at 632.8nm. The red areas represent the relative high points, and blue represent the relative low points on the surface.

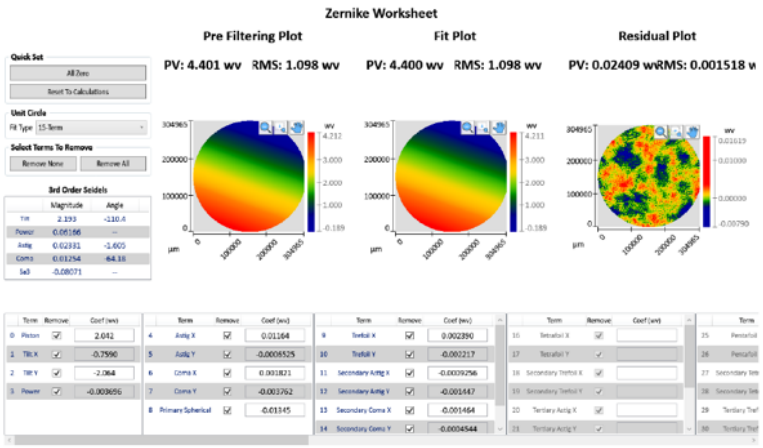

Figure 36: Zernike Worksheet with Pre-Filtering Plot, Fit Plot, and Residual Plot

In addition, the Zernike data was extracted (See Fig 36). Here, they are used to describe the shape of the aberrated wavefront in the pupil of an optical system, specifically this mount for a 330mm transmission flat. In precision optical manufacturing, such as these high precision transmission flats, they are used to characterize higher order aberrations present in the transmitted wavefront of the optic. This is done by fitting the wavefront slopes to the polynomial derivatives averaged over a particular aperture in order to deduce the magnitude of the aberrations in the wavefront. For this pre-assembled flat that has been polished to such a tight surface figure, the aberrations present in the wavefront are minimal, as would be required for a reference caliber optic.

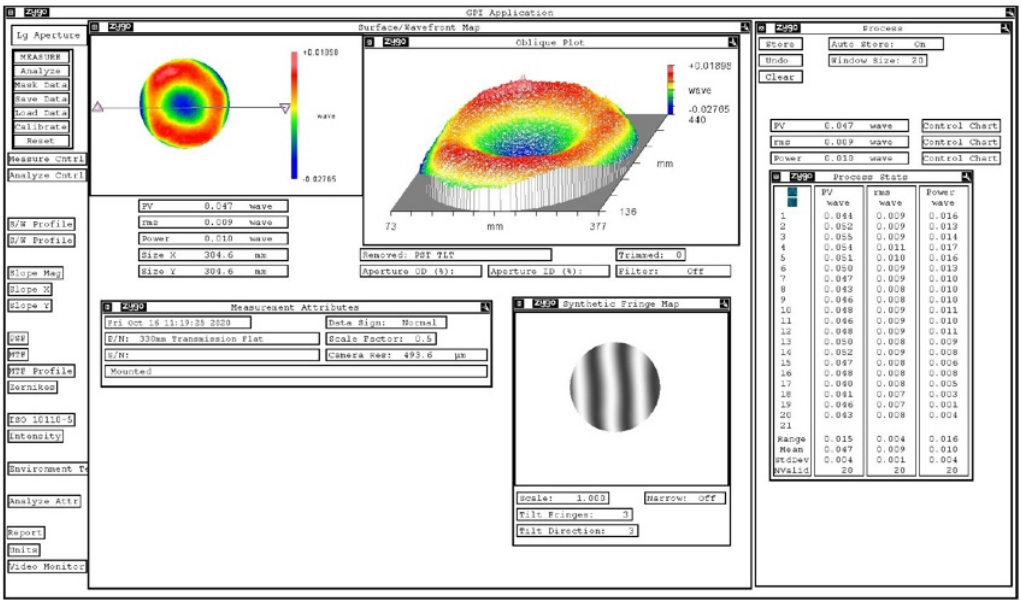

Figure 37: Post Assembly Data, Transmitted Wavefront Error Through the Substrate at 0.047 waves at 632.8nm

Having minimal observable aberrations, such as astigmatism, in a reference quality optic is beneficial because it reduces the error from the surface form of the reference optic appearing in the data of the components being tested. Often times during the set-up process after installing the reference optic onto the testing system, in this case a beam-expanded interferometer, a 'sub-traction' file needs to be created in order to normalize the data by removing and power and/or irregularity from the testing data. Having a more randomized surface figure on the reference optic creates a more uniform data set when it is used to asses other components, giving more confidence to the quality assurance technician that if they observe a defect in their data when testing an optical component, that the defect is actually occurring on the part being tested, and not an error induced by the reference optic.

Figure 38: Zernike Data of Post assembly substrate, with the Pre -Filtering Plot, Fit Plot, and Residual Plot

Another consideration is that the wedge in the optic was oriented at the three-o'clock to nine-o'clock axis (x-axis), and was maintained throughout the testing process from the in-process measurements to the final quality assurance step when the substrate was mounted into the assembly.

5. Discussion

In addition, the data appears that the pressure from the compression rubber is more uniform around the substrate, as can be seen in the interferograms. In the adhesive method, the source of the adhesive stress can clearly be seen in three locations, which produces an uneven distribution in the stress profile (See Fig. 37). A more even distribution makes it easier to compensate by creating a subtraction file of the surface figure of the flat. When compared with FEA analysis of the displacement analysis, it can be seen that there is little correlation between the two showing similar stress rings in both the interferometric and FEA displacement profiles.

When comparing the two Zernike worksheets, the results are confirmed for both pre and post assembly operation, the Zernike data also shows that the average difference between the pre and post assembly difference was approx. 0.0105 waves (See Fig. 38). Which at 632.8nm would be the equivalent of approx. 6.6nm. This shows that the changes due to the stresses that were induced by the assembly process changed on average by less than one-hundredth of a wave, which correlates to the FEA diagrams showing a lack of induced stress in the assembly.

Although the interferograms appear to show a donut shaped surface figure, the numerical data suggests that the surface is more uniform than the image suggest. The figure does indicate that the weighting was concentrated in the center of the substrate when it was on the polishing lap. This is done primarily during the early stages of the polishing process, when the goal is to ensure that the full surface is specular, and there is no more diffuse area of the surface left (at least outside of the clear aperture).

Based on the stiffness and displacement analysis, the results suggest that both were negligible to the final performance of the mounted substrate in the assembly. 6061 T6 aluminum, is a very strong material, and the load that is being subjected to it from the transmission flat is not a big load considering the material. When doing the opto-mechanical analysis of the system (modeling the system as a set of springs in series), the natural frequency was shown to be 4.462hz and the active damping performed by the air table. Looking at the roughness lambda/100 difference between the mounted substrate and the unmounted substrate, it is unlikely that the natural frequency of the system had any contribution to the overall system. Whether this is due to a damping effect that was created by the vibration resistant rubber pads on the system has not been explored, however, since a detailed analysis of this has not been done, the pad may have also contributed to either a higher frequency or provided more damping. However, the approx.

one percent difference between the surface figure of the substrate before-and-after, indicates that any contribution would be negligible.

6. Conclusions and Future Work

Often times, these interferometers are used in a shop environment, rather than a laboratory environment. These shop environments are often an area of high activity, and often times equipment, such as Fizeau interferometers, can be damaged, as well as undergoing long-term wear-and tear due to continuous use in a shop environment. This often necessitates that the primary transmission flat needs to be repolished and recoated, which requires the system to be disassembled in order to perform the repair, and then reassembled once the repairs are complete. Often times, such as with the 100mm diameter flat described earlier, the need to remove and reapply a low-outgassing adhesive (low outgassing needed as a mitigating to potentially contaminating the anti-reflective coating) which adds another level of difficulty that increases the risk of damaging the substrate to a point beyond simple repair, and would require replacement (a much more expensive option).

The repair process, although standardized through years of internal industrial knowledge, can be a delicate process, especially for the tight optical tolerances that are required to be used as reference quality optics. As described earlier, the polished process could take on the order of several weeks, with multiple rounds of in-process quality control in order to achieve the surface figure and wavefront error needed.

Therefore, an adhesive free approach, such as the one that is demonstrated by the mount, mitigates this issue by removing the complicated process of removing and reapplying adhesive. In addition, for an adhesive to work properly, there needs to be an amount of tension in-order to provide sufficient grip in order to secure the flat, often through metal-to-metal contact. The

adhesive free method displayed here removes that tension, with the primary forces acting on the substrate primarily being force due to gravity.

Despite these major changes into a standard mount design, the data show that on average there was less than $1/90^{th}$ of a wave difference (approx. 7nm at 632.8nm wavelength) between the unassembled substrate and the fully assembled substrate using the adhesive free mount. This demonstrates that this approach is a viable alternative in-order to preserve the optical properties needed for the transmission flat for a Fizeau interferometric application, while greatly simplifying the long-term servicing and repair.

Another area of improvement is the simplification of the top engagement pad. When observing both the interferometric and FEA data, it showed that there was little to any significant force that was being applied by the top engagement pad. The original intention of the top engagement pad was to provide down force in the y-axis direction in order to provide more stability for the transmission flat when mounted in the assembly. Removal of the pad will likely be a cost reduction, and smooth out the complexity of the entire build. The FEA data shows that it's the two lower engagement pad that are bearing the brunt of the load (as expected), and distributes the force well enough to not cause major stress for the system as seen comparing the pre and post assembly interferometric data. For revision two of the mount, the top structure of the pad in order to keep the assembly structurally together would still be needed, but the engagement pad does not need to be added.

One place in which it would be interesting to put in future research is the exploration of a hybrid method, in which minimal adhesive is used at some locations and the rubber resistance pads are used in another location. Even though the adhesive free approach has a lot of advantages, the adhesive mount approach does have the advantage of simplifying some of the mounting

apparatus. The engagement pads consist of over a dozen parts, some of them are small. The assembly of the pads themselves can be a tricky exercise, since we are using a combination of extension and compression spring, fighting again the forces of both to assemble the pads can be difficult. An adhesive injection method, although it likely will be a messy process, will certainly reduce the cost of manufacturing. The two primary pieces of the engagement pad were CNC machined as custom components. This is certainly a cost driver, as customer components are usually much more expensive then off the shelf ones (such as the spring and dowel pins purchased from McMasterCarr). An adhesive method would reduce this complexity by reducing the need to build more custom CNC components than need be, it can both reduce the time and cost of building the mount.

Another approach for the testing would be to perform an absolute measurement using the three flat testing method. In our case, the surface figure of the reference flat was provided at lambda-20 PV at 632.8nm. Our initial measurements showed that the wavefront figures were beyond that in the lambda/27 PV at 632.8nm range. A general rule of thumb you can only measure to an accuracy of the testing tool you are using. In interferometric metrology, one way around this to measure the wavefront and surfaces of optical components is to use a three-flat testing method. Three-flat tests are a type of measurement procedure that separates errors in the interferometer reference wavefront from errors due to the test part surface, this is a so-called absolute test.[38] Although a subtraction file for the reference flat that was sold with the Zygo system, and a flat-field subtraction file for the camera was included that mitigates some of the issues without doing

[38] Ulf Griesmann, "Three-flat test solutions based on simple mirror symmetry," Appl. Opt. 45, 5856-5865 (2006) https://opg.optica.org/ao/abstract.cfm?URI=ao-45-23-5856

a three-flat test, an absolute measurement would also be interesting to observe to compare and contrast the results.

From an opto-mechanical standpoint, also observing the change in the natural frequency of the system when also adding the large tip-tilt stage and the vibration pads in the z-axis direction would make it a complete exercise. However, since there was no visible indication that the natural frequency (whether damped by the vibration resistant pads or not) would lead to a different result in the overall system. All optics needs to be set on top of something during the quality assurance process, and it would be an exercise going down a rabbit hole to account for everything. A further complete study that also examine whether the rubber pads on the engagement pad assembly was either contributing or damping the natural frequency of the system, could be done to better understand what effects that such a feature would contribute.

Finally, it would be interesting to observe the change in wavefront error through the optic when the assembly is being subjected to different temperatures. For example, measuring the change in the wavefront and/or surface figure when outside of standard conditions. This currently assembly was designed to be used in a quality assurance/lab environment. However, if it can be shown and tested that the assembly would also perform well in both hotter and colder condition, it would make it more likely that this assembly could also be used in a manufacturing floor situation, which would allow the technicians to test and make adjustment to the polishing conditions, such as changing the pH of the polishing compound, or adjusting the weighting of the flat during initial polishing sequence.

Finally, if there were a compilation of data sets, and a thorough analysis of the requirements between reference quality optics and more standard components, an objective set of guidelines could be generated that would assist in systems engineers to better determine what specifications

are needed for various applications, such as metrology, astronomy, or semi-conductor applications, rather than relying on word of mouth or trial and error to choose the correct specification for their optical component.

Appendix:

This appendix is an excel file calculator using eq. 8, 9, to calculate the stiffness of the fused silica transmission flat.

Parameter	*Formula*	*Raw Val*	*Units*	*Useful Val*	*Units*	*Physical Meaning*
Material Properties of Fused Silica						
E1		72	GPa	72000000000	Pa	Young's Modulus, Fused Silica
v1				0.17	-	Poisson's Ratio, Fused Silica
α_l				0.5	ppm/K	CTE, Fused Silica
ρ_1m				2200	kg/m^3	Mass Density
ρ_1w				21582	kg/m^3*N	Weight Density
Material Properties of Aluminum, Al6061-T6						
E2		68	GPa	68000000000	Pa	Young's Modulus, Al
v2				0.33	-	Poisson's Ratio, Al
α_2				23.6	ppm/K	CTE, Al
rho_2				2.7	kg/m^3	Density, Al
Transmission Flat Geometry						
r		165	mm	0.165	m	Mirror Aperture Diameter
RoC		100000000	mm	100000	m	Radius of Curvature (Flat)
t		50	mm	0.05	m	Thickness of Mirror
Volume		1069123.25	mm^2	0.001069123	m^3	Total Volume
Mass				2.35207115	kg	Total Mass
Fg				23.07381798	N	Concentrated Force of Gravity
Gravity Sag						
gamma	=r^2/(2*t*RoC)			2.7225E-06	-	Schwesinger Factor
Ck, two pt support				0.054660758	-	, two pt support
delta_rms, two pt support		**0.89213942**	nm	**8.92139E-10**	m	Two-Point Supported Deflection
Stiffness Estimation						
k_mirr	=Fg/delta_rms	**25863.4665**	N/um	25863466465	N/m	First Order Stiffness under self-deflection load

Aluminum Pad Stiffness					
Parameter	Val	Units	Useful Val	Units	Physical Meaning
E	68.9	GPa	68900000000	Pa	Young's Modulus, Al6061-T6
t	22.0429	mm	0.0220429	m	Thickness
w_arc	90.012	mm	0.090012	m	Width
A			0.001984126	m^2	Cross Sectional Area
L	8.696	mm	0.008696	m	Length of Leg Unit
k_aluminum	15720589693	N/m	15720.58969	N/um	Stiffness of Single Blade Unit
Rubber Pad Stiffness					
E	1	MPa	1000000	Pa	Young's Modulus, 50 Shore Hardness, Neoprene
t	22.0429	mm	0.0220429	m	
w_arc	90.012	mm	0.090012	m	
A	1984.125515	mm^2	0.001984126	m^2	
L	3.175	mm	0.003175	m	
k_rubberPad	0.624921422	N/um	624921.422	N/m	
COTS Spring Stiffness					
k_spring	373480.315	N/m	440	lbf/in	Aluminum Stiffness
Single Leg Stiffness					
k_leg	233765.9985		0.233765998	N/um	Entire Series Axial Stiffness of Leg
theta_strut	30	deg	0.523598776	rad	(Half Angle)
k_bipod_vertical	0.350648998	N/um	0.350648998	N/um	
k_bipod_tangential	0.116882999	N/um	0.116882999	N/um	
Translational Stiffness					
Position Angle 1	0	deg	0	rad	
Position Angle 2	120	deg	2.094395102	rad	
Position Angle 3	240	deg	4.188790205	rad	
	kx	ky	kz	Units	
Bipod 1	0			N/um	
Bipod 2	0.087662249	0.02922075	0.350648998	N/um	
Bipod 3	0.087662249	0.02922075	0.350648998	N/um	
Totals	0.175	0.058	0.701	N/um	
Solution	0.175324499	0.175324499	1.051946993	N/um	
	decenter	out of page	(vertical motion)		
Rotational Stiffness					
	KTx	Kty	KTz		
Totals	N/A	N/A	N/A	N*um/um	
Solution	N/A	N/A	N/A		

References:

1. Golini, D., Kordonski, W. I., Dumas, P., & Hogan, S. J. (1999). Magnetorheological finishing (MRF) in commercial precision optics manufacturing. *Optical Manufacturing and Testing III*. doi:10.1117/12.369174
2. Hooper, A. R., Hoffmann, N. N., Sarkas, H. W., Escolas, J., & Hobbs, Z. (2015). Deterministic polishing from theory to practice. *Optifab 2015*. doi:10.1117/12.2196055
3. Kim, D., Aftab, M., Trumper, I., Graves, L., Quach, H., Kang, H., . . . Choi, H. (2019). Programmatic Large Precision Optics Manufacturing. *INTERNATIONAL CONFERENCE ON OPTICS AND ELECTRO-OPTICS (ICOL 2019)*.
4. Netterfield, R., Oreb, B., Leistner, A., Green, K., Seckold, J., & Gross, M. (2005). Manufacturing and testing of precision optical components - from substrate to coating and assembling. *Optical Fabrication, Testing, and Metrology II*. doi:10.1117/12.625539
5. Parks, R. E. (1982). Overview Of Optical Manufacturing Methods. *Contemporary Methods of Optical Fabrication*. doi:10.1117/12.932708
6. Xie, R., Zhao, S., Liao, D., Chen, X., Wang, J., Xu, Q., . . . Jiang, Z. (2019). Recent advances in rapid polishing process of large aperture optical flats. *9th International Symposium on Advanced Optical Manufacturing and Testing Technologies: Meta-Surface-Wave and Planar Optics*. doi:10.1117/12.2505131
7. Yellowhair, J., Su, P., Novak, M., & Burge, J. (2007, August 28). *Fabrication and Testing of Large Flats*. Lecture presented in College of Optical Sciences University of Arizona, Tuscon.Title of Site. Available online: URL (accessed on Day Month Year).

8. Herzog, H., Segal, J., Smith, J., Bates, R., Calis, J., De La Torre, A., . . . Wicker, R. (2015). Optical fabrication of lightweighted 3D printed mirrors. *Proceedings of SPIE, 9573*(957308), 15th ser. doi:10.1117/12.2188197

9. Graves, L. R., Smith, G. A., Apai, D., & Kim, D. W. (2019). Precision Optics Manufacturing and Control for Next-Generation Large Telescopes. *Nanomanufacturing and Metrology, 2*(2), 65-90. doi:10.1007/s41871-019-00038-2

10. James E. Millerd, Neal J. Brock, John B. Hayes, James C. Wyant, "Instantaneous phase-shift point-diffraction interferometer," Proc. SPIE 5531, Interferometry XII: Techniques and Analysis, (2 August 2004); doi: 10.1117/12.560959

11. Sasian, J. M., North-Morris, M., Wruck, G. L., Williby, G. A., & Greivenkamp, J. E. (1999). Rock and roll polishing: A process for optical surface polishing. *SPIE: Optical Engineering, 38*(12).

12. Brock, N., Hayes, J., Kimbrough, B., Millerd, J., North-Morris, M., Novak, M., & Wyant, J. C. (2005). Dynamic interferometry. *Novel Optical Systems Design and Optimization VIII*. doi:10.1117/12.621245

13. Kimbrough, B., Millerd, J., Wyant, J., & Hayes, J. (2006). Low-coherence vibration insensitive Fizeau interferometer. *Interferometry XIII: Techniques and Analysis*. doi:10.1117/12.682956

14. Millerd, J., Brock, N., Hayes, J., Kimbrough, B., North-Morris, M., & Wyant, J. C. (2017). Vibration insensitive interferometry. *International Conference on Space Optics — ICSO 2006*. doi:10.1117/12.2308094

15. Morris, M. N., Naradikian, M., & Millerd, J. (2010). Noise reduction in dynamic interferometry measurements. *Interferometry XV: Techniques and Analysis*. doi:10.1117/12.860450

16. Michael B. North-Morris, James E. Millerd, Neal J. Brock, John B. Hayes, "Phase-shifting multiwavelength dynamic interferometer," Proc. SPIE 5531, Interferometry XII: Techniques and Analysis, (2 August 2004); doi:10.1117/12.560829

17. Zhou, P., & Burge, J. (2010). Diffraction Effects in Interferometry. *OSA / IODC/OF&T 2010*.

18. Brock, N., Kimbrough, B. T., & Millerd, J. E. (2011). A pixelated micropolarizer-based camera for instantaneous interferometric measurements. *Polarization Science and Remote Sensing V*. doi:10.1117/12.896608

19. Cai, W., Kim, D., Zhou, P., Parks, R. E., & Burge, J. (2010). Interferometer Calibration using the Random Ball Test. *OSA / IODC/OF&T 2010*.

20. Kim, D. W., Aftab, M., Trumper, I. L., Graves, L. R., Quach, H., Kang, H., . . . Choi, H. (2020). Reconfigurable dynamic optical system design, test, and data analysis. *Optics and Photonics for Advanced Dimensional Metrology*. doi:10.1117/12.2555650

21. Kim, D. W., Aftab, M., Choi, H., Graves, L., & Trumper, I. (2016). Optical Metrology Systems Spanning the Full Spatial Frequency Spectrum. *Frontiers in Optics 2016*. doi:10.1364/fio.2016.fw5g.4

22. Guo, X., Zeng, A., & Huang, H. (2008). Spatial phase-shifting lateral shearing interferometer. *2008 International Conference on Optical Instruments and Technology: Optoelectronic Measurement Technology and Applications*. doi:10.1117/12.806931